

3550

NACA TN 2124

0065361



TECH LIBRARY KAFB, NM

NATIONAL ADVISORY COMMITTEE FOR AERONAUTICS

TECHNICAL NOTE 2124

SPECTRUMS AND DIFFUSION IN A ROUND TURBULENT JET

By Stanley Corrsin and Mahinder S. Uberoi

The Johns Hopkins University



Washington

July 1950

TECH

AFMTC

319-98/41



TABLE OF CONTENTS

| | Page |
|---|------|
| SUMMARY | 1 |
| INTRODUCTION | 1 |
| SYMBOLS | 4 |
| EQUIPMENT | 7 |
| Aerodynamic Equipment | 7 |
| Measuring Equipment | 8 |
| PROCEDURES | 10 |
| Velocity Spectrum | 10 |
| Temperature Spectrum | 10 |
| Shear-Correlation Spectrum | 11 |
| Velocity Correlation Function | 12 |
| Temperature Correlation Function | 12 |
| Mean Temperatures behind Local Source | 12 |
| Temperature Fluctuations behind Local Sources | 12 |
| EXPERIMENTAL RESULTS | 13 |
| Shear-Correlation Spectrum | 13 |
| Velocity and Temperature Spectrums | 13 |
| Transverse Correlation Functions | 14 |
| Mean Thermal Wakes behind Local Heat Sources | 14 |
| Temperature Fluctuations behind Local Heat Source | 16 |
| ANALYSIS OF RESULTS | 16 |
| Shear-Correlation Spectrum | 16 |
| Velocity and Temperature Spectrums | 17 |
| Transverse Correlation Functions | 22 |
| Mean Thermal Wakes behind Local Heat Sources | 23 |
| DISCUSSION | 26 |
| Local Isotropy | 26 |
| Velocity and Temperature Spectrums | 28 |
| Kinematic and Thermal Scales | 28 |
| Transverse Correlation Functions | 29 |

TABLE OF CONTENTS

| | Page |
|---|------|
| Probability Density of $v(t)$ and $w(t)$ | 30 |
| Temperature Fluctuations behind Local Heat Source | 31 |
| Sources of Error | 32 |
| SUMMARY OF RESULTS | 32 |
| APPENDIX A - HEAT LOSS FROM A WIRE AT VARIOUS AMBIENT TEMPERATURES | 34 |
| APPENDIX B - MEASUREMENT OF SHEAR-CORRELATION SPECTRUM | 36 |
| REFERENCES | 41 |

NATIONAL ADVISORY COMMITTEE FOR AERONAUTICS

TECHNICAL NOTE 2124

SPECTRUMS AND DIFFUSION IN A ROUND TURBULENT JET

By Stanley Corrsin and Mahinder S. Uberoi

SUMMARY

In a round turbulent jet at room temperature, measurement of the shear correlation coefficient as a function of frequency (through band-pass filters) has given a rather direct verification of Kolmogoroff's local-isotropy hypothesis.

One-dimensional power spectrums of velocity and temperature fluctuations, measured in unheated and heated jets, respectively, have been contrasted. Under the same conditions, the two corresponding transverse correlation functions have been measured and compared.

Finally, measurements have been made of the mean thermal wakes behind local (line) heat sources in the unheated turbulent jet, and the order of magnitude of the temperature fluctuations has been determined.

INTRODUCTION

At the present time there apparently exists no statistical theory of turbulent shear flow. One significant theoretical consideration has been proposed: The hypothesis of local isotropy, originated by Kolmogoroff (references 1 and 2). Kolmogoroff has suggested that the fine structure in turbulent shear flow may be isotropic; recent experiments of Townsend (references 3 and 4) in a turbulent wake seem to verify this hypothesis.

In view of this situation, the various experimental researches in the field follow two courses: First, they attempt to verify or disprove local isotropy; second, they try in all conceivable ways to make measurements that may shed light upon the basic nature of the turbulent shear flow, so that the foundations for a successful theory can be laid.

During recent years it has become evident that measurements of the intensity of turbulence alone cannot provide sufficient information about the statistical and dynamical properties of the flow fields. Such quantities as correlations, spectrums, probability densities, the various terms in the turbulent kinetic-energy balance, and so forth may be expected to reveal many essential features of the problem.

The types of turbulent shear flow that have come under close experimental scrutiny are the boundary layer (references 5 and 6), the plane channel (reference 7), the plane wake (references 3 and 4), the plane single free-mixing region (reference 8), and the round jet (references 9 and 10). The present work is a continuation of that reported in references 9 and 10.

The general objectives of this investigation have been to learn something more about the flow in a fully developed round turbulent jet and about the heat transfer in such a flow. The work reported here has fallen into three phases: (a) An attempt to establish the presence or absence of local isotropy, (b) a comparison of velocity- and temperature-fluctuation fields when the over-all boundary conditions on mean velocity and temperature are effectively the same, and (c) a study of the diffusion of heat from a local (line) source in the turbulent flow.

The only specific experimental verification of local isotropy in a turbulent shear flow to date was by Townsend in the plane wake behind a circular rod (references 3 and 4). He found that the skewness and flattening factors of the probability density of $\partial u / \partial t$ in the shear flow are very closely equal to those in the (effectively isotropic) turbulence far behind a grid. Since differentiation emphasizes the higher frequencies, his measurement shows, in essence, that the values of certain statistical quantities related to the smaller eddies in a shear flow are the same as the values for the smaller eddies in isotropic turbulence. He also found the microscale of u in the stream direction to be nearly $\sqrt{2}$ times the microscale of v in that direction, a relation which is exactly true for isotropic turbulence.

Until recently, only mean-velocity and mean-temperature distributions were measured to provide a comparison of the transfer rates of momentum and of heat in turbulent shear flows with over-all heat transfer. The previous report in this round-jet investigation (reference 10) included a beginning on the problem of direct comparison of the velocity and temperature fluctuations as well as some measurements of velocity-temperature correlations. The fluctuations in a warm turbulent wake have been studied by Townsend.¹

Up to the present time, however, there appears still to be no successful hypothesis to account for the well-known fact that heat (and other scalar quantities, like material) is diffused more rapidly than momentum in a turbulent flow. Thus, more detailed study of the fluctuations seemed in order.

¹Private communications, 1949.

The first real analysis on the diffusive property (for scalar quantities) of a homogeneous turbulent field was Taylor's well-known work, "Diffusion by Continuous Movements" (reference 11).

The mean thermal wake behind a line source of heat in a flowing isotropic turbulence has been carefully measured by Schubauer (reference 12) in the region close to the source, and by Simmons (measurements reported in reference 13) over an extended range. Taylor's theory of diffusion by continuous movements is directly applicable to the diffusion from a line source of heat in a homogeneous turbulent field, and he has made a generalization to permit application of the method in a decaying isotropic turbulence (reference 13).

In a turbulent shear flow, the only published measurements of the thermal wake of a local source seem to be those of Skramstad and Schubauer in a turbulent boundary layer.² These were reported by the experimenters (reference 14) and by Dryden (reference 15). The temperature distribution across the wake in shear flow is decidedly skew. On the other hand, in the isotropic turbulence, it is to all intents and purposes a Gaussian curve. Of course, in a homogeneous field this curve (measured close enough to the source so that the Lagrangian correlation coefficient is still effectively unity) is simply the probability density of the lateral velocity fluctuations. This relation may be roughly true for shear flow as well, in which case the contrasting results mentioned above would mean that the probability density of $v(t)$ is skew in shear flow, but Gaussian in decaying isotropic turbulence.

No measurements had been made of the fluctuations in these thermal wakes, and it was felt that some information on the nature of these might help further a general understanding of the diffusive process.

This investigation was conducted at the Aeronautics Department of the Johns Hopkins University under the sponsorship and with the financial assistance of the National Advisory Committee for Aeronautics. The authors would like to acknowledge many stimulating conversations with Dr. L. S. G. Kovasznay, and to thank Dr. F. H. Clauser for his helpful criticism. Donation of the hot-jet unit by Dr. C. B. Millikan, Director of the Guggenheim Aeronautical Laboratory at the California Institute of Technology, is greatly appreciated. Mr. Philip Lebowitz helped to set up much of the laboratory equipment.

²Wieghardt has recently measured the diffusion of heat from a local source in a turbulent boundary layer (reference 16), but his source was flush with the solid surface and thus he was studying a different problem, that is, one more directly related to micrometeorological conditions.

SYMBOLS

| | |
|--|---|
| d | diameter of orifice (1 in.) |
| x | axial distance from orifice |
| r | radial distance from jet axis |
| \bar{U} | axial component of mean velocity |
| \bar{V} | radial component of mean velocity |
| \bar{W} | tangential component of mean velocity |
| \bar{U}_{\max} | maximum \bar{U} at a cross section on axis |
| u | axial component of instantaneous velocity fluctuation |
| v | radial component of instantaneous velocity fluctuation |
| w | tangential component of instantaneous velocity fluctuation |
| $u' \equiv \sqrt{u^2}$ | |
| $v' \equiv \sqrt{v^2}$ | |
| θ | instantaneous temperature difference (measured <u>above room temperature as reference</u>) |
| $\bar{\theta}$ | mean temperature difference (measured <u>above room temperature as reference</u>) |
| $\bar{\theta}_{\max}$ | maximum mean temperature difference at a cross section |
| $\bar{\theta}_0$ | maximum mean temperature in jet at orifice |
| ϑ | instantaneous temperature fluctuation ($\equiv \theta - \bar{\theta}$) |
| $\vartheta' \equiv \sqrt{\vartheta^2}$ | |
| t | time |
| e | voltage fluctuation |
| α, β | sensitivity of a diagonal hot-wire to u and to v , respectively |

| | |
|----------------------------|---|
| R_{uv} | shear correlation coefficient $(\overline{uv}/u'v')$ |
| u_n, v_n | instantaneous contributions of $u(t)$ and $v(t)$, respectively, in a narrow frequency band of nominal frequency n ; in a Fourier series discussion, the n th harmonic of periodic $u(t)$ and $v(t)$, respectively |
| $u_n' \equiv \sqrt{u_n^2}$ | |
| $v_n' \equiv \sqrt{v_n^2}$ | |
| nR_{uv} | shear correlation coefficient for a narrow band of frequencies $(\overline{u_n v_n}/u_n' v_n')$; this function is referred to as the "shear-correlation spectrum" or, briefly, the "shear spectrum" |
| ϕ, ψ | phase angles |
| $n^F u, n^F v$ | in Fourier series analysis, $n^F u \equiv a_n^2 / \sum_1^\infty a_n^2$, $n^F v \equiv b_n^2 / \sum_1^\infty b_n^2$, where a_n and b_n are Fourier series coefficients |
| n | cyclic frequency in general; in particular, magnitude of radial coordinate in three-dimensional frequency space |
| n_1 | cyclic frequency of one-dimensional spectrums of $u(t)$ and $\vartheta(t)$ |
| k | wave-number magnitude for three-dimensional spectrums $(2\pi n/\bar{U})$ |
| k_1 | wave-number magnitude for one-dimensional spectrums $(2\pi n_1/\bar{U})$ |
| k_0 | a reference constant with dimensions of wave numbers |
| $F_1(k_1)$ | one-dimensional power spectrum of $u(t)$ in terms of wave number |
| $F_1^*(n_1)$ | one-dimensional power spectrum of $u(t)$ in terms of frequency |

| | |
|----------------------|--|
| $F(k)$ | three-dimensional power spectrum of velocity fluctuation |
| $G_1(k_1)$ | one-dimensional power spectrum of $\vartheta(t)$ in terms of wave number |
| $G_1^*(n_1)$ | one-dimensional power spectrum of $\vartheta(t)$ in terms of frequency |
| $G(k)$ | three-dimensional power spectrum of temperature fluctuation |
| R_y | transverse correlation function of u measured symmetrically about jet axis $(\overline{u_1 u_2} / \overline{u^2})$ |
| R_x | longitudinal correlation function of u |
| S_y | transverse correlation function of ϑ measured symmetrically about jet axis $(\overline{\vartheta_1 \vartheta_2} / \overline{\vartheta^2})$ |
| L_x | longitudinal scale of u -fluctuations |
| Λ_x | longitudinal scale of ϑ -fluctuations |
| L_y | lateral scale of u -fluctuations |
| Λ_y | lateral scale of ϑ -fluctuations |
| λ_x | longitudinal microscale of u -fluctuations |
| λ | lateral microscale of u -fluctuations |
| l | lateral microscale of ϑ -fluctuations |
| l_x | longitudinal microscale of ϑ -fluctuations |
| ξ | distance downstream from local heat source in x -direction |
| ζ | lateral distance, perpendicular to source line, from local heat source |
| ϕ | dimensionless temperature ratio $(\overline{\theta} / \overline{\theta}_{\max})$ |
| $\eta = \zeta / \xi$ | |
| Δ | standard deviation of mean-temperature distribution in wake behind local heat source |
| τ | pulse spacing |

h pulse height
j pulse width

EQUIPMENT

Aerodynamic Equipment

The 1-inch hot-jet unit is shown schematically in figure 1. The centrifugal blower is driven by a 1/2-horsepower direct-current motor. Heat is added through two double banks of coils of No. 16 Nichrome wire. As can be seen in the sketch, a good part of the heated air is directed around the outside of the jet-air pipe in order to maintain a flat initial temperature distribution in the jet. A vacuum-cleaner blower is used to help the air through this secondary heating annulus, and this warm air is fed back into the intake of the main blower.

The section of relatively high velocity between heaters and final pressure box permits adequate mixing behind the grid, to insure thermally homogeneous initial jet air.

Figure 2 is a photograph of the unit as set up previously (reference 10); the present arrangement is essentially the same.

All turbulence measurements were made with an initial jet total head in the range from 3.5 to 5.0 inches of water. In free turbulent flows there is no detectable effect of jet Reynolds number over a much wider range of Reynolds numbers than this.

When the jet was run unheated, there was a slight temperature rise through the blower and duct. In the measurements of thermal wake behind a local heat source, correction for this ambient-temperature field was unnecessary. For all hot runs, the orifice air temperature was very close to 200° C, about 175° above room temperature.

Three different "local heat sources" were used:

- (a) A straight diametrically strung wire of 0.008-inch Nichrome
- (b) A 2-inch-diameter Nichrome ring
- (c) A 4-inch-diameter Nichrome ring

Because of the extremely high turbulence levels encountered in a free jet, a measurable thermal wake could only be obtained by using source temperatures in the range from 300° to 700° C. This undoubtedly led to

some local buoyancy effects, but, even with this order of temperatures, the thermal wake was barely detectable 1 inch downstream.

The Reynolds numbers of these heat-source wires were about as follows:

For straight wire on axis,

150, based on air temperature
22, based on wire temperature

For 2-inch-diameter ring,

110, based on air temperature
16, based on wire temperature

For 4-inch-diameter ring,

59, based on air temperature
9, based on wire temperature

No noticeable additional turbulence was generated by these wires, and no average momentum defect could be detected with a flattened total-head tube, even as close as $1/4$ inch downstream.

Measuring Equipment

The measuring instruments used were: Total-head tube, Chromel-Alumel thermocouple, and hot-wire anemometer (also used as resistance thermometer).

The hot-wires were nominally 0.000635-centimeter platinum, about 1.5 millimeters in length, etched from Wollaston wire. The etched platinum was soft-soldered to the tips of small steel needle supports. A discussion of heat loss from a wire at various ambient temperatures is given in appendix A.

The basic hot-wire-anemometry equipment was purchased from Mr. Carl L. Thiele of Altadena, California. One of the two identical heating circuits is shown in figure 3.

The amplifier, with resistance-capacitance compensation network, is given in figure 4. The uncompensated gain is constant to within ± 2 percent over a frequency range from 3 to 12,000 cycles per second (fig. 5). With the wires and operating conditions used (time constants on the order of 1 millisecond), the over-all compensated response was good over the same range. Correct setting of the compensation network was determined by superimposing a square wave upon the hot-wire bridge

(reference 17). Unfortunately, in a free turbulent shear flow the ambient disturbance is so great (because of the extremely high turbulence levels) that calibration cannot be made in the flow to be studied.

The vacuum-thermocouple signal output was measured either with a millivoltmeter or by the average deflection rate of a fluxmeter.

The various spectrums reported here were measured with a modified General Radio Type 760-A Sound Analyzer (reference 18). The changes in output stage (fig. 6) were made to eliminate the direct-current component and to obtain linear instead of logarithmic response. As modified, the sound analyzer had rather undesirable frequency-response characteristics, particularly a day-to-day shift in relative amplification of the higher-frequency ranges. The frequency-response calibration in figure 7 is plotted in terms of voltage squared, since this was the quantity ultimately measured.

The frequency pass band for this analyzer is far from the optimum rectangular shape. However, the slopes of the two sides are sufficiently steep that no appreciable error is attributable to noninfinite slopes, with the spectrums measured in this investigation. Figure 8 is an experimentally determined band shape. There was fair similarity of band shape over the entire frequency range. For computational purposes, an equivalent rectangular pass band was defined as indicated in the figure.

The instrument is a type recording constant-percent band width, measuring the product of power spectrum times frequency. This has obvious advantages in the high-frequency range where there is so little turbulent energy.

Possibly the chief disadvantage of the actual band shape is the extremely sharp peak, causing a great deal of fluctuation in the output signal, and making any simple meter-reading technique virtually impossible in the low- and medium-frequency ranges. Consequently an integrating technique was devised, making use of the negligible restoring-torque characteristics of a Sensitive Research Company fluxmeter. The integrating technique used is shown schematically in figure 9. Actually a bank of vacuum thermocouples was used, and the resistances shown are just typical values. The signal put out by the thermocouples is a highly fluctuating direct current.

The bucking circuit was necessitated by the following combination of requirements:

(a) For the lowest frequencies reasonable consistency could be obtained only by integrating over periods as long as 3 minutes

(b) Appreciable static bearing friction in the fluxmeter demanded more or less continuous motion of the needle

(c) The restoring torque of the fluxmeter is no longer negligible in the range of very large deflection. Hence it was desirable to keep total deflection to a minimum.

Thus, most of the average direct-current component of the thermocouple signal was bucked out, and the constant bucking current was read on a precision microammeter. The fluxmeter needle fluctuated more or less about the zero-deflection point during the time of integration, and its reading at the end of this time ordinarily gave a small correction on the result.

In the highest-frequency range, overload considerations on the sound analyzer limited the signal drastically, and only a part of the thermocouple direct current was bucked.

For the determination of average wake temperatures behind the local heat sources, the thermocouple voltage was measured with a Leeds & Northrup type K-2 potentiometer.

Oscillograms were taken from a blue oscilloscope tube by means of a General Radio Type 651-AE camera, using fast film.

PROCEDURES

Velocity Spectrum

The power (or energy) spectrum of the longitudinal velocity fluctuations at a point in the unheated jet was measured by conventional hot-wire-anemometry technique, with a continuously adjustable band-pass filter, as described under EQUIPMENT.

Temperature Spectrum

The power spectrum of the temperature fluctuations in the heated jet was measured by using the hot-wire effectively as a simple resistance thermometer (reference 19). The amplified voltage signal was analyzed exactly as in the measurement of velocity spectrums.

Shear-Correlation Spectrum

For the shear-correlation spectrum, the quantity to be measured is the correlation coefficient between a narrow frequency band of u -fluctuations and the same narrow frequency band of v -fluctuations, at the same point in the flow field.

The method, for any particular nominal frequency, was to pass the various voltage signals (e_1 , e_2 , $e_1 + e_2$, $e_1 - e_2$) from an X-type shear- (or v' -) meter through the band-pass filter after amplification. By appropriate combination of the mean-square values of these four signals (identical with total-shear measurement), there results

$${}_n R_{uv} \equiv \overline{u_n v_n} / u_n' v_n'$$

where the subscript n indicates the narrow band of nominal frequency n cycles per second. A justification for the validity of this procedure is obtainable by considering the two velocity-fluctuation components as periodic functions. Of course, this is not a real proof.

If a symmetrical X-meter is assumed, the two instantaneous voltage signals are

$$\left. \begin{aligned} e_1 &= \alpha u + \beta v \\ e_2 &= \alpha u - \beta v \end{aligned} \right\} \quad (1)$$

For periodic fluctuations,

$$\left. \begin{aligned} u &= \sum_{n=1}^{\infty} a_n \cos (2\pi n t + \phi_n) \\ v &= \sum_{n=1}^{\infty} b_n \cos (2\pi n t + \psi_n) \end{aligned} \right\} \quad (2)$$

In this simple case, the correlation coefficient for any spectral line is merely

$${}_n R_{uv} = \cos (\phi_n - \psi_n) \quad (3)$$

If equations (2) are substituted into equations (1), it is easily shown that

$$\cos (\phi_n - \psi_n) = \frac{\overline{n e_1^2} - \overline{n e_2^2}}{\sqrt{\overline{n(e_1 + e_2)^2} \overline{n(e_1 - e_2)^2}}} \quad (4)$$

in complete analogy to the conventional method for measuring R_{uv} with an x-meter. The algebraic details are given in appendix B.

When the meter is not perfectly symmetrical ($\alpha_1 \neq \alpha_2$; $\beta_1 \neq \beta_2$), the formal processes, both algebraic and experimental, become excessively involved. Consequently, in actual practice the effect of unavoidable unsymmetry in the x-meter was essentially nullified by taking double sets of readings at each frequency, rotating the instrument 180° about the axis of flow direction between sets.

Velocity Correlation Function

The double correlation R_y between longitudinal velocity fluctuation at pairs of points on opposite sides of the jet axis was measured only in the unheated jet. Hence the standard hot-wire-anemometry technique was used. The two hot-wires were always equidistant from the axis (on a diameter), so that they were under identical operating conditions.

Temperature Correlation Function

In the hot jet, the wires traversing symmetrically as for R_y were operated as simple resistance thermometers, so that the double temperature correlation S_y could be determined directly.

Mean Temperatures behind Local Source

To determine mean temperatures behind a local source, traverses were made with a Chromel-Alumel thermocouple, whose voltage was measured with a Leeds & Northrup type K-2 potentiometer.

Temperature Fluctuations behind Local Sources

To determine temperature fluctuations behind local sources, the fine platinum wire was operated at small currents, so that it worked essentially as a resistance thermometer.

EXPERIMENTAL RESULTS

Mean-velocity and mean-temperature distributions for various orifice temperatures are presented in reference 10.

Shear-Correlation Spectrum

The spectrum of shear correlation coefficients $nR_{uv} = \overline{u_n v_n} / \overline{u_n} \overline{v_n}$ was measured in the unheated jet at $x/d = 20$ at a radial station corresponding to maximum shear at this cross section. Figure 10 shows quite definitely that $nR_{uv}(n)$ is a function decreasing monotonically to zero. Thus, the hypothesis of local isotropy is seen to be verified in a very direct way. The value of the directly measured total-shear correlation coefficient $R_{uv} = \overline{uv} / \overline{u} \overline{v}$ is indicated in the figure.

Velocity and Temperature Spectrums

The one-dimensional power spectrum $F_1(k_1)$ of the longitudinal velocity fluctuations $u(t)$ was measured at two radial positions in the unheated jet, at $x/d = 20$. Figure 11 gives the two spectrums, one measured on the axis, and one measured at about the maximum-shear location. Plotted against wave number $(k_1 = 2\pi\eta/\bar{U})$, the two spectrums are identical within the experimental scatter. The solid line drawn as approximation to the points is made up as follows:

- (a) For $0 < k_1 < 1.25$, it is Von Kármán's semiempirical formula (reference 20):

$$F_1\left(\frac{k_1}{k_0}\right) = \frac{\text{Constant}}{\left[1 + \left(\frac{k_1}{k_0}\right)^2\right]^{5/6}} \quad (5)$$

- (b) For $k_1 > 1.25$, a nonanalytical curve has been faired in

The Von Kármán expression was used primarily to simplify the problem of extrapolation to $k_1 = 0$ and to shorten the work of transformation to three-dimensional spectrums. (See "Velocity and Temperature Spectrums" under ANALYSIS OF RESULTS.)

The corresponding one-dimensional power spectrums of temperature fluctuations $G_1(k_1)$ were measured in the heated jet ($\theta_0 = 170^\circ \text{C}$) at $x/d = 20$. One spectrum is on the jet axis; one is at about the

radial station of maximum heat transfer (and shear). From figure 12, it can be seen that they differ noticeably in the high-frequency range, but are essentially identical in the low- and moderate-frequency ranges. The curves used to approximate the experimental points are as follows:

On the axis - the Von Kármán formula is used over the entire range

At the maximum-heat-transfer point -

(a) For $0 < k_1 < 1.0$, the Von Kármán formula is used

(b) For $k_1 > 1.0$, a nonanalytical curve has been faired in

Figures 13 and 14 contrast velocity spectrums with temperature spectrums at corresponding radial stations.

Transverse Correlation Functions

The double correlation function $R_y = \overline{u_1 u_2} / u_1' u_2'$, measured symmetrically about the axis at $x/d = 20$ in the unheated jet, is plotted in figure 15. Of course, since the wires are in identical flow conditions, $u_1' = u_2' = u'$ (say), and $R_y = \overline{u_1 u_2} / u^2$.

The double correlation function $S_y = \overline{\vartheta_1 \vartheta_2} / \vartheta_1' \vartheta_2'$ in the heated jet at $x/d = 20$ is plotted in figure 16. Since this was also measured symmetrically, $S_y = \overline{\vartheta_1 \vartheta_2} / \vartheta^2$, where $\vartheta_1' = \vartheta_2' = \vartheta'$ (say).

Clearly, the range of measurable temperature correlation exceeds the range of measurable velocity correlation by an amount greater than can be attributed simply to the fact that the hot jet is wider than the unheated jet (reference 10).

Mean Thermal Wakes behind Local Heat Sources

Typical radial distributions of average temperature behind a straight (diametrical) wire, a 2-inch-diameter ring, and a 4-inch-diameter ring at $x/d = 20$ in the unheated jet are shown in figures 17, 18, and 19, respectively. The points in these figures are not direct experimental points, but merely serve to indicate the faired results for different distances downstream. All these have been corrected for the previously mentioned small ambient-temperature field in the unheated jet. There was rather large scatter (illustrated only in fig. 20) due to the small temperature differences measured and to the extremely large degree of fluctuation present. The 4-inch ring is slightly outside of the fully turbulent jet core (reference 9); consequently the results for

this case are not of direct interest in a study of fully developed turbulence. The figures show that each of the thermal wakes possesses similarity well within the accuracy of measurement.

All of the thermal wakes spread linearly in the measured range (figs. 21, 22, and 23). From Taylor's theory of diffusion by continuous movements, this simply indicates that, for the maximum downstream station studied, the Lagrangian correlation coefficient of the v-fluctuations has still not departed appreciably from unity.

For a straight-line source at the jet axis, because of conservation of heat, it follows immediately from similarity and linear spread that the maximum temperature at a cross section in the wake $\bar{\theta}_{\max}$ must decrease hyperbolically with increasing downstream distance. Let $\bar{\theta}/\bar{\theta}_{\max} = \Phi(\eta)$, where $\eta = \xi/\delta$ and δ is some characteristic width of the wake, for example, the ξ at which $\Phi = 1/2$; conservation of heat gives

$$\int_0^{\infty} \bar{\theta} d\xi = \text{Constant} \quad (6)$$

where the mean-velocity changes are neglected. Then,

$$\bar{\theta}_{\max} \delta = \text{Constant}/I_1 \quad (7)$$

where

$$I_1 = \int_0^{\infty} \Phi(\eta) d\eta$$

The same is true of the annular wake in the range of ξ so small that $\delta \ll r$.

Single traverses were also made behind a straight-line heat source for two other cases:

(a) With the line source set perpendicular to r at a radius of 1 inch, a temperature traverse was made in the r -direction, at $\xi = 1/2$ inch (fig. 24)

(b) With the line source set on a diametral line, a temperature traverse was made perpendicular to r at a radius of 1 inch; $\xi = 1/2$ inch (fig. 25)

Temperature Fluctuations behind Local Heat Source

As can be anticipated, the temperature fluctuations close behind a local heat source are quite different in nature from the velocity fluctuations at the same point or from the temperature and velocity fluctuations in a turbulent flow with over-all heat transfer. Since a suitable source produces no additional turbulence,³ the velocity fluctuations should be the same as in undisturbed flow. On the other hand, the "turbulent" thermal wake close to the source must be simply a very narrow laminar thermal wake which is fluctuating in direction as $v(t)$ fluctuates. Since all of the fluid outside of this unsteady laminar wake is of constant temperature and the temperature fluctuations can only be positive, the general character of the oscillogram of $\vartheta(t)$ in figure 26 is understandable. These records were taken about $3/8$ inch downstream from the straight-line heat source, and about $3/16$ inch off the wake axis. All of the oscillograms were made with insufficient compensation for the hot-wire thermal lag, in order to suppress the (high frequency) noise and thus permit the basic form of $\vartheta(t)$ to stand out. From these two oscillograms of $u(t)$ and check measurements of the turbulence levels for the two cases, it appears that the source wire has made no appreciable change in the turbulence.

Measurements of the intensity of the temperature fluctuations across a section at $\xi = 0.4$ inch are given in figure 27. In the same vicinity the values of u'/\bar{U} and v'/\bar{U} are on the order of 20 percent. The extremely high values of $\vartheta'/\bar{\theta}$ are not surprising since the mean temperature difference is due only to the presence of the fluctuation. Since the simple-resistance-thermometer theory is based upon the assumption of small fluctuations compared with absolute temperature (reference 19), it is expected that these measurements are about as accurate as the measurements of much lower $\vartheta'/\bar{\theta}$ in the hot jet (reference 10).

ANALYSIS OF RESULTS

Shear-Correlation Spectrum

A very convenient check upon the shear-spectrum measurements can be gotten by the simple expedient of computing the total (or "net") turbulent shear correlation coefficient (which was also directly measured) from this spectrum and the turbulent-energy spectrum. Again, an elementary Fourier series treatment serves to justify (not prove)

³An ideal source would also produce no average momentum defect. However, as mentioned previously, the momentum wakes of the local sources were relatively so small as to be completely undetectable as close as $1/4$ inch downstream.

the intuitive idea that the total correlation coefficient R_{uv} is simply a weighted average of the nR_{uv} (i.e., the cosines of the phase angles), weighted simply by the product of the square roots of the energy spectrums of u and v . The calculation is given in appendix B, and yields the relation

$$R_{uv} = \sum_{n=1}^{\infty} (nF_u nF_v)^{1/2} nR_{uv} \quad (8)$$

Unfortunately, 25 cycles per second is the lower limit of the measured frequency range, so that some extrapolation must be made to lower frequencies which contain much of the turbulent energy. Since no theoretical basis yet exists to guide this extrapolation (like the Von Kármán formula in the case of energy spectrums), guesses had to be made as to the maximum and minimum of reasonable-looking extrapolation curves. These are plotted in figure 28, along with the energy spectrum of the u -fluctuations. Since no spectrum of the v -fluctuations was measured, the expression actually used for computing R_{uv} is

$$R_{uv} = \int_0^{\infty} F_1(k_1) k_1 R_{uv} dk_1 \quad (9)$$

The best of the three extrapolations tried (extrapolation (3)) gives $R_{uv} = 0.46$, which is satisfactorily close to the directly measured value of 0.44, especially since there is no reason to suppose that the spectrum of the v -fluctuations is identical with the spectrum of the u -fluctuations, except in the range of local isotropy.

Velocity and Temperature Spectrums

The one-dimensional spectrums of velocity and temperature fluctuations, as plotted in figures 11 and 12, respectively, are area-normalized; that is, they are defined such that

$$\int_0^{\infty} F_1(k_1) dk_1 = 1.0 \quad (10)$$

$$\int_0^{\infty} G_1(k_1) dk_1 = 1.0 \quad (11)$$

However, the original measurements were made on an absolute-value basis, so that the total fluctuation levels u'/\bar{U} and $\vartheta'/\bar{\theta}$ could be used as checks on the spectrums. The spectrums as measured were $F_1^*(n_1)$ and $G_1^*(n_1)$, defined such that, ideally,

$$\int_0^{\infty} F_1^*(n_1) \, dn_1 = \overline{u^2} \quad (12)$$

$$\int_0^{\infty} G_1^*(n_1) \, dn_1 = \overline{\vartheta^2} \quad (13)$$

Integration of F_1^* as indicated in equation (12) yielded the following:

On the axis ($r = 0$),

$$\frac{1}{\bar{U}} \left(\int_0^{\infty} F_1^* \, dn_1 \right)^{1/2} = 0.28$$

($u'/\bar{U} = 0.22$, directly measured)

In the maximum-shear region ($r = 4.0$ cm),

$$\frac{1}{\bar{U}} \left(\int_0^{\infty} F_1^* \, dn_1 \right)^{1/2} = 0.52$$

($u'/\bar{U} = 0.40$, directly measured)

Similar integration of the measured temperature spectrum in the heated jet yielded the following:

On the axis ($r = 0$),

$$\frac{1}{\bar{\theta}} \left(\int_0^{\infty} G_1^* \, dn_1 \right)^{1/2} = 0.21$$

($\vartheta'/\bar{\theta} = 0.18$, directly measured)

In the maximum-shear region ($r = 4.8$ cm),

$$\frac{1}{\bar{\theta}} \left(\int_0^\infty G_1^* dn_1 \right)^{1/2} = 0.41$$

$$(\vartheta'/\bar{\theta} = 0.36, \text{ directly measured})$$

On the jet axis, where conventional small-perturbation hot-wire theory may still be moderately accurate, the agreement is satisfactory.

It should be noted in passing that these directly measured values of $\vartheta'/\bar{\theta}$ are appreciably higher than those reported in reference 10. No explanation for this difference is apparent.

The longitudinal scale of u -fluctuations is obtainable approximately from the power spectrum:

$$L_x = \frac{\pi}{2} F_1(0) \quad (14)$$

which follows from the fundamental Fourier transformation,

$$F_1(k_1) = \frac{2}{\pi} \int_0^\infty R_x \cos(k_1 x) dx \quad (15)$$

in the limit $k_1 \rightarrow 0$.

An analogous treatment of a temperature-fluctuation field leads to an identical expression for the longitudinal scale of ϑ -fluctuations:

$$\Lambda_x = \frac{\pi}{2} G_1(0) \quad (16)$$

Within the accuracy of measurement, the longitudinal scale of $u(t)$ was found to be the same on the jet axis and in the maximum-shear region:

$$L_x = 3.6 \text{ centimeters}$$

The same was true of the longitudinal temperature scales in the hot jet:

$$\Lambda_x = 2.4 \text{ centimeters}$$

In all these computations the measured spectrums were extrapolated to zero wave number with a parabola, as first suggested by Dryden (reference 21). Approximately the same numerical values are obtained with the Von Kármán formula illustrated in the plotted curves.

In order to compare L_x in the unheated jet with Λ_x in the heated jet, L_x may be multiplied by 1.15, the jet-width ratio at $x/d = 20$ for these two initial temperatures (reference 10). The "corrected" L_x is then 4.15 centimeters.

It must be recalled that the Fourier transformation relation between time spectrum and space correlation would be exactly true only if the turbulent fluctuations at a point were due to pure rectilinear translation (by \bar{U}) of a fixed fluctuation pattern. For the free jet flow, the extremely high turbulence levels make such a transformation very uncertain. Therefore, equations (14) and (16) (and the resulting scales) can only be considered as crude approximations.

The longitudinal microscale,

$$\lambda_x = \left[-\frac{2}{R_x''(0)} \right]^{1/2} \quad (17)$$

may also be computed approximately from the one-dimensional power spectrum, by

$$\frac{1}{\lambda_x^2} = \frac{1}{2} \int_0^\infty k_1^2 F_1(k_1) dk_1 \quad (18)$$

(Primes signify differentiation when applied to correlations and spectrums.)

Again, an analogous approach to temperature fluctuations gives

$$\frac{1}{\lambda_x^2} = \frac{1}{2} \int_0^\infty k_1^2 G_1(k_1) dk_1 \quad (19)$$

Unfortunately, the high-frequency ranges of the G_1 's are too uncertain to permit reasonable extrapolation and the use of equation (19), although it can be seen from figure 13 that $\lambda_x > l_x$. However, equation (18) has been used to compute the longitudinal velocity microscale. Figure 29 is a plot of the integrand of equation (18). The integration and appropriate computation give

$$\lambda_x = 0.44 \text{ centimeter}$$

and the same value for both radial positions.

Since the turbulence on the axis of such a jet seems to be rather isotropic (the experimental evidence is that $\overline{uv} = 0$ and $u' \approx v'$), the lateral microscale

$$\lambda = \left[-\frac{2}{R_y''(0)} \right]^{1/2} \quad (20)$$

is of the order of $\lambda_x/\sqrt{2}$; that is,

$$\lambda \approx 0.31 \text{ centimeter}$$

With the assumption of isotropic turbulence on the jet axis, it is possible to compute the three-dimensional power spectrum $F(k)$ from the one-dimensional spectrum $F_1(k_1)$. Heisenberg (reference 22) has given the inverse transformation

$$F_1(k_1) = \frac{1}{4} \int_{k_1}^{\infty} \frac{F(k)}{k^2} (k^2 - k_1^2) dk \quad (21)$$

and the desired $F(F_1)$ is readily found to be

$$F(k_1) = 2k_1 [k_1 F_1''(k_1) - F_1'(k_1)] \quad (22)$$

A three-dimensional spectrum computed in this way is given in figure 30.

The corresponding spectral transformations for the three-dimensional isotropic fluctuation field of a scalar quantity (temperature, for example) are simply (reference 23)

$$G_1(k_1) = \frac{1}{2} \int_{k_1}^{\infty} \frac{G(k)}{k} dk \quad (23)$$

and

$$G(k_1) = -2k_1 G_1'(k_1) \quad (24)$$

With the assumption of isotropic temperature fluctuations on the jet axis, equation (24) has been used to compute $G(k)$.

The three-dimensional velocity and temperature spectrums on the jet axis are very nearly the same - provided that the isotropy assumption is reasonably good. The curve in figure 30, which shows the general nature of both F and G , is simply the transformation of the Von Kármán approximations to F_1 and G_1 .

It must be recalled, however, that F_1 is in the unheated jet, while G_1 is in the heated jet. Although the results of references 9 and 10 indicate no essential change in the detailed dynamics of jet turbulence as a result of moderate increase in jet temperature, there is an appreciable increase in jet width at a given x/d . As mentioned earlier, the width ratio between $\bar{\theta}_0 = 175^\circ$ and $\bar{\theta}_0 = 0^\circ$ is about 1.15 at $x/d = 20$.

Transverse Correlation Functions

The integral area under the velocity correlation function (fig. 15) may be considered to give a sort of lateral scale of turbulence in the jet, although the result is not associated with any particular region in the jet. The conventional expression,

$$L_y = \int_0^{\infty} R_y(r) dr \quad (25)$$

gives a scale, $L_y = 0.67$ centimeter.

If a lateral temperature scale is defined in similar fashion,

$$\Lambda_y = \int_0^{\infty} S_y(r) dr \quad (26)$$

then for the heated jet at $x/d = 20$ it turns out that $\Lambda_y = 0.77$ centimeter from the function as given in figure 16.

Appropriate comparison of these transverse scales may be had if L_y is multiplied by the jet-width ratio: $1.15L_y = 0.77$ centimeter, the same value as Λ_y . However, the two correlation functions that yield these net areas are still quite different in shape. The contrast is shown in figure 31. Clearly, even though the net areas are identical, there is nonzero temperature correlation over appreciably greater distances.

A rough approximation to the microscale of turbulence can be gotten by guessing at the osculating parabola for $\Delta r = 0$. In this particular case "guessing" is more appropriate than "fitting," since the job is entirely extrapolatory in nature. Figure 32(a) shows the vertex region of R_y with the parabola that corresponds to

$$\lambda = \left[-\frac{2}{R_y''(0)} \right]^{1/2} = 0.28 \text{ centimeter} \quad (27)$$

This value is in surprisingly good agreement with the 0.31 centimeter obtained from the power spectrum on the axis. In fact, the agreement must be regarded as fortuitous, since the difference is appreciably less than the experimental uncertainty.

If the temperature-fluctuation field is again considered analogously, the transverse microscale of temperature fluctuations (fig. 32(b)) is

$$\lambda = \left[-\frac{2}{S_y''(0)} \right]^{1/2} = 0.43 \text{ centimeter} \quad (28)$$

For comparison, $1.15\lambda = 0.32$.

Mean Thermal Wakes behind Local Heat Sources

The rate of spread of the thermal wake close behind a local source of heat was first used by Schubauer (reference 12) as a means of

measuring the intensity of lateral velocity fluctuations v'/\bar{U} . A detailed discussion of this technique has been given by Taylor (reference 13) and need not be repeated here. The results of such a computation, compared with direct X-meter measurements of v'/\bar{U} , are as follows:

| r (in.) | $\left(\frac{v'}{\bar{U}}\right)_{\text{wake}}$ | $\left(\frac{v'}{\bar{U}}\right)_{\text{X-meter}}$ |
|--------------|---|--|
| 0 | 0.18 | 0.185 |
| 1 | .22 | .20 |
| 2 | .40 | .30 |

The X-meter measurements were corrected for the effects of both u' and uv upon the slightly unsymmetrical meter.

It is possible to get some additional information about the fluctuation field by computation from the turbulent-heat-transfer equation. In particular, an estimate of the distribution $\overline{\vartheta v}$ across a section of the thermal wake behind the line source may be made as follows.

The steady turbulent-heat-transfer equation for low velocity (negligible viscous dissipation to heat), negligible molecular heat conduction, and constant density is, in Cartesian tensor notation,

$$\bar{U}_i \frac{\partial \bar{\theta}}{\partial x_i} = - \frac{\partial}{\partial x_k} (\overline{\vartheta u_k}) \quad (29)$$

For the region in the immediate vicinity of the jet axis, assume that conditions approximate those in a homogeneous field of turbulence; that is, $\bar{V} = \bar{W} = 0$ and $\bar{U} = \text{Constant} = \bar{U}_{\text{max}}$.

Then equation (29) becomes simply

$$\bar{U}_{\text{max}} \frac{\partial \bar{\theta}}{\partial \xi} \approx - \frac{\partial}{\partial \xi} (\overline{\vartheta u}) - \frac{\partial}{\partial \zeta} (\overline{\vartheta v}) \quad (30)$$

The assumption of small turbulence level implies $\overline{\vartheta u} \ll \overline{\theta} \overline{U}_{\max}$ and hence

$$\overline{U}_{\max} \frac{\partial \overline{\theta}}{\partial \xi} \approx - \frac{\partial}{\partial \xi} (\overline{\vartheta v}) \quad (31)$$

This would be a good approximation in turbulence far behind a grid placed in a uniform stream, but is certainly rather crude here.

The final assumption, that of similarity in the thermal wake, is well supported by the experimental results. Then let

$$\frac{\overline{\theta}}{\overline{\theta}_{\max}} = f\left(\frac{\xi}{\Delta}\right) \equiv f(\eta) \quad (32)$$

where Δ is the standard deviation of the mean-temperature distribution, and, according to the theory of diffusion by continuous movements, is therefore proportional to the standard deviation of the probability density of $v(t)$ as well. Specifically, for a small ξ in a homogeneous turbulent flow,

$$\Delta = \frac{v'}{\overline{U}} \xi \quad (33)$$

Similarity also implies that

$$\overline{\vartheta v} = \overline{\theta}_{\max} \overline{U}_{\max} \omega(\eta) \quad (\text{say}) \quad (34)$$

Equation (7) may be written

$$\overline{\theta}_{\max} \Delta = \text{Constant} \quad (7a)$$

Then, with equations (32), (34), and (7a), equation (31) may be transformed to

$$\frac{d\omega}{d\eta} = \frac{d\Delta}{d\xi} \frac{d}{d\eta} (\eta f) \quad (35)$$

or, with equation (33),

$$\frac{d\omega}{d\eta} = \frac{v'}{\overline{U}_{\max}} \frac{d}{d\eta} (\eta f) \quad (36)$$

Since v'/\bar{U}_{\max} is constant in this approximation,

$$\omega(\eta) = \frac{v'}{\bar{U}_{\max}} \eta f(\eta) + \text{Constant}$$

and the boundary condition, $\omega = 0$ at $\eta = 0$, gives finally

$$\frac{\overline{\partial v}}{\bar{\theta}_{\max} \bar{U}_{\max}} = \frac{v'}{\bar{U}_{\max}} \frac{\xi}{\Delta} \frac{\bar{\theta}}{\bar{\theta}_{\max}} \quad (37)$$

which is conveniently written in the form

$$\frac{\overline{\partial v}}{\bar{\theta}_{\max} \bar{U}_{\max}} = \frac{\bar{\theta}}{\bar{\theta}_{\max}} \frac{\xi}{\xi} \quad (38)$$

In figure 33 this function is plotted against ξ/ξ for the traverse 1/2 inch downstream from the straight-wire heat source, across the jet center.

DISCUSSION

Local Isotropy

The monotonic decrease to zero in shear correlation coefficient with increasing frequency seems to be decisive evidence for the existence of local isotropy at sufficiently high Reynolds numbers. It is interesting to note that the spectral region of negligible shear ($n_1 > 1000$ cps in the present particular determination, for example) contains only about 1.5 percent of the turbulent kinetic energy in u^2 . Of course, this is by no means an indication of the importance of the existence of local isotropy in a turbulent shear flow. A more pertinent comparison would be with figure 29, which shows in effect dissipation as a function of frequency. From this it appears that about 90 percent of the dissipation of turbulent kinetic energy to heat takes place in essentially isotropic turbulence. This permits the use of the Taylor expression for dissipation in isotropic turbulence (reference 24). Of course it also implies that the isotropic relation between longitudinal and lateral microscales, $\lambda_x = \sqrt{2}\lambda$, will be fairly accurate even in the region of high turbulent shear. Furthermore, it implies a

universal dimensionless spectral function for all turbulent flows, in the high-frequency region. For turbulence at this Reynolds number, it appears that a universal part of the spectrum exists only for $k_1 > 7.9$, which is well beyond the point of slope $-\frac{5}{3}$. In fact, the " $-\frac{5}{3}$ point" in this spectrum is just at $k_1 = 1.0$.

At this point a few remarks on the appropriate type of measurement for verification of local isotropy may be in order. In particular, a careful distinction must be made between the shear spectrum nR_{uv} as presented in this report and the power spectrum of the randomly fluctuating quantity uv which might be measured with a multiplying circuit followed by a frequency analyzer.

Local isotropy specifies that restriction to a sufficiently small domain in a turbulent shear flow shows up isotropy in the various statistical properties that are studied within that domain. It implies that all three components of the frequency (or wave-number) vector must be large, and not merely the magnitude of the vector. Clearly then a good indication of isotropy is zero correlation between orthogonal velocity-fluctuation components; this means that the highest-frequency parts of u , v , and w are uncorrelated with each other. Hence it is clear that if $\overline{u_n v_n}$ decreases to zero, with increasing frequency, faster than the product $u_n' v_n'$ decreases to zero, local isotropy exists. In terms of coefficient, this merely requires that nR_{uv} decrease to zero eventually.

Now consider the fluctuating quantity uv . In a turbulent shear flow $\overline{uv} \neq 0$, so that uv consists of a direct-current component with superimposed random fluctuations. Since the conventional electronic techniques eliminate the direct current, the quantity to be analyzed would be $uv - \overline{uv}$ as a function of time. If local isotropy were present, the lower frequencies of u and v would be rectified in the multiplying process, and therefore the oscillogram and power spectrum of $uv - \overline{uv}$ would have relatively great emphasis on the high frequencies. In other words, if the naively measured power spectrum of uv were used as an indication of local isotropy, it would show a trend opposite to that of $\overline{u_n v_n}$; that is, it would decrease more slowly than the product $u_n' v_n'$. In general, the measurement of nR_{uv} seems like a much more specific and direct approach than the measurement of the power spectrum of uv . Presumably, a (somewhat more complicated) Fourier series discussion like that in appendix B could also be carried out for the power spectrum of uv .

Velocity and Temperature Spectrums

The apparent identity of the velocity power spectrums $F_1(k_1)$ on the jet axis and in the region of maximum shear is only approximate and has been determined only down to $k_1 = 0.1$. There still exists the possibility of measurable divergence in the lowest wave-number range. The good degree of agreement indicates that, in diffusing from the region of maximum production (near the maximum-shear region) to the region of maximum dissipation (on the jet axis), the turbulent kinetic energy has not done any gross migrating in the wave-number space.

On the other hand, the apparent decided difference between temperature power spectrums measured on the axis and in the maximum-heat-transfer region seems to indicate such a migration. However, the considerable scatter at the highest measured frequencies renders definite conclusions impossible.

Somewhat more specific conclusions can be drawn from the comparison between one-dimensional velocity and temperature spectrums. On the jet axis, for example, in spite of distinct differences between these two spectrums, it turns out that within the experimental scatter (which is considerable) the three-dimensional power spectrums may be much more nearly identical. The fact that they did in fact come out to be identical over a wide range of wave number when computed from the empirically fitted Von Kármán formula must certainly be regarded as pure chance. This is true not only because of the experimental uncertainty, but also because these spectrums were measured in two similar but different flows, whose characteristic lengths probably differed by 15 percent.

Kinematic and Thermal Scales

From the extrapolated zero-wave-number intercepts of the one-dimensional spectrums, the following longitudinal scales were obtained at $x/d = 20$:

$$L_x = 4.15 \text{ centimeters}$$

$$\Lambda_x = 2.4 \text{ centimeters}$$

This L_x is 15 percent greater than the unheated-jet value, to allow for the greater width of the heated jet. Thus, $L_x/\Lambda_x = 1.7$. In a homogeneous, isotropic field of velocity and temperature fluctuations, it turns out (reference 23) that, if the three-dimensional power spectrums of velocity and temperature are proportional, $L_x/\Lambda_x = 1.50$.

It may also be noted that, if the measured ratio were in an isotropic field, $L_y = \frac{1}{2}L_x$ and $\Lambda_y = \Lambda_x$, so that $L_y/\Lambda_y = 0.85$. The ideal value would be 0.75. Actually, the integrals of the transverse correlation functions R_y and S_y are considerably less than the scales that would be expected, according to these relations, in a homogeneous isotropic turbulence.

On the other hand, the relative values of longitudinal and lateral kinematic microscales follow the isotropic relation, $\lambda_x = \sqrt{2}\lambda$, at least within the experimental uncertainty. This is on the order of ± 25 percent in the case of the parabola "fitted" at the vertex of R_y .

Unfortunately, the temperature spectrum on the jet axis is not extended sufficiently far to permit computation of longitudinal microscale l_x there. The spectrums in figure 13 show only that l_x is considerably less than λ_x ; that is, l_x is considerably less than 0.44 centimeter. It may be remarked in passing that isotropy for a scalar quantity means equality of longitudinal and lateral correlation functions. The lateral microscale, $l = 0.43$ centimeter, obtained by "fitting" a parabola at the vertex of S_y seems of reasonable magnitude relative to $1.15\lambda = 0.32$ centimeter.

Transverse Correlation Functions

Of course, the reason L_y and Λ_y as determined by integration of functions R_y and S_y are not related isotropically to L_x and Λ_x is that over most of the range of Δr the probes are in decidedly non-isotropic turbulence. Thus, there is no reason to expect $L_y = \frac{1}{2}L_x$ or $\Lambda_y = \Lambda_x$, when L_x and Λ_x are computed from the spectrums.

An examination of the behavior of these two symmetrically measured correlation functions shows that there is nonzero correlation over a considerable part of the jet, but that the relatively small scales result from the rather extensive regions of negative correlation. This behavior is emphasized by a comparison of R_y with the corresponding function in some typical isotropic turbulence downstream of 1-inch-mesh grid (reference 25). Figure 34 shows the contrast clearly.

It is conceivable that such an extended region of negative correlation is characteristic of turbulent shear flow. However, until someone establishes this in a shear flow whose transverse extent is very large compared with the maximum correlation distance, it may be safer to guess that the "excess" amount of negative correlation is simply due to a slight irregular waving of the jet as a whole. In reference 9 it

was assumed that, since R_y actually goes to zero at large values of Δr , there is no over-all "whipping" of the jet. However, such a conclusion does not appear to be completely warranted.

In the section entitled "Transverse Correlation Functions" under ANALYSIS OF RESULTS, it was found that in the heated jet $L_y \approx \Lambda_y$. On the other hand, it is well known that the lateral rate of transfer of heat is appreciably greater than the lateral rate of transfer of momentum, as was first found by Ruden (reference 26) from mean-velocity and mean-temperature measurements. Since diffusion is essentially Lagrangian in nature, while L and Λ are Eulerian scales, the above results are not necessarily in contradiction. The appreciably greater distance over which $S_y \neq 0$ (as contrasted with R_y) may, however, be related to the fact that the mean thermal jet diameter is appreciably greater than the mean momentum jet diameter.

Probability Density of $v(t)$ and $w(t)$

The mean-temperature distribution close behind the straight-line heat source on the jet axis is effectively symmetrical, and closely resembles a Gaussian curve in shape (fig. 20); this shows that the probability density of $v(t)$ on the axis is more or less Gaussian, as in isotropic turbulence.

The mean-temperature distributions close behind the two ring heat sources are decidedly skew. However, some of this skewness seems to be due simply to the curvature of the line sources. Therefore, the temperature distribution across the wake of a straight wire set tangent to the circle $r = 1$ inch was measured. Neglecting the effects of mean-velocity gradient, this curve (fig. 24) is proportional to the probability density of the radial velocity fluctuation $v(t)$ in the shear region. It is seen to be slightly skew; the skewness factor

$$S \equiv \frac{\overline{v^3}}{(\overline{v^2})^{3/2}} \approx -0.1$$

is computed directly from this curve. The thermal wake measurements of Skramstad and Schubauer behind a line source in a turbulent boundary layer (reported in reference 15) show a skewness of 0.38. The differences in sign and magnitude of these two skewness factors suggest lateral turbulence-level gradient as the cause. The gradients in v'/\bar{U} are of opposite sign in these two flows.

Calculation from figure 25 shows that the probability density of the tangential fluctuation $w(t)$ is symmetrical. It may be noted that on the axis of such an axially symmetric flow there is no distinction between radial and tangential velocity fluctuation; hence figure 20 also applies to $w(t)$ on the axis.

Temperature Fluctuations behind Local Heat Source

The extremely high temperature-fluctuation levels ($\vartheta'/\bar{\theta} > 1.0$) encountered in the wake of the line heat source are easily understood from a brief consideration of the nature of the temperature field. Close behind the source, there is just a single narrow laminar thermal wake which is being blown in random deviations from the ξ -direction by the turbulent fluctuations. The gross turbulent thermal wake is simply the wedge-shaped region over which this relatively narrow wake wanders. Hence the total thermal signal at any fixed point in the gross wake consists simply of a series of pulses, where each pulse corresponds to an occasion upon which the laminar wake swept over the point. Obviously, the frequency of occurrence of pulses will decrease monotonically with increasing transverse distance from the center of the gross wake.

If this type of temperature signal is represented schematically by periodic square pulses of height h , width j , and fundamental wave length τ (fig. 35), then it can be easily deduced that the fluctuation level is

$$\frac{\vartheta'}{\bar{\theta}} = \sqrt{\frac{\tau}{j} - 1}$$

where it is recalled that $\vartheta = \theta - \bar{\theta}$ by definition.

Two pulse spacings of interest are

$$(1) \tau = 2j; \text{ then } \vartheta'/\bar{\theta} = 1.0$$

$$(2) \tau \rightarrow \infty; \text{ then } \vartheta'/\bar{\theta} \rightarrow \infty$$

Hence, the measured results for $\vartheta'/\bar{\theta}$ seem quite reasonable in both order of magnitude and in qualitative behavior across the gross thermal wake of the local heat source.

The distribution of $\overline{\vartheta v}/\bar{\theta}_{\max} \bar{u}_{\max}$ computed from the thermal wake, plus the availability of the measurements of $\vartheta'/\bar{\theta}_{\max}$ and v'/\bar{u}_{\max} , suggests the computation of the heat-transfer correlation coefficient $\overline{\vartheta v}/\vartheta'v'$. Unfortunately, when the results of figures 33 and 27

are used, a part of the correlation-coefficient distribution reaches impossible values (slightly above unity). It must be concluded that the absolute values of $\overline{v}/\overline{\theta}_{\max}\overline{U}_{\max}$ are too inaccurate for such a computation.

Sources of Error

Aside from the specific instances mentioned earlier in this section, the sources of experimental error are much the same as outlined on pages 27 to 28 of reference 10. Additional uncertainties arise in the spectrum measurements, especially in the higher-frequency range, because of (a) rapid changes in the calibration of the sound analyzer (band peak response against frequency, fig. 7) and (b) slight static friction of fluxmeter bearings.

In general, it should be emphasized that measurements by conventional (small-perturbation) hot-wire anemometry in a flow of this high level of turbulence cannot be considered as accurate absolute-value measurements. Even on the jet axis, where the level is a minimum and conditions are relatively steady, there is no reason to believe that absolute values are better than within, say, ± 10 percent of the "correct" values. However, relative behaviors are undoubtedly determined, and dimensionless measures of the type of correlation coefficients are more accurate than absolute values.

None of the measurements reported here have been corrected for finite length of hot-wires.

SUMMARY OF RESULTS

From measurements in a round turbulent jet at room temperature of the shear correlation coefficient as a function of frequency, of velocity and temperature fluctuations with and without jet heating, and of the mean thermal wakes behind local heat sources, the following statements may be made:

1. The Kolmogoroff hypothesis of local isotropy is verified for the shear flow in a round turbulent jet. This is concluded from the monotonic decrease to zero of the shear-correlation spectrum $(\overline{u_n v_n}/\overline{u_n' v_n'})$ with increasing frequency n .
2. The one-dimensional power spectrums of longitudinal velocity fluctuations and of temperature fluctuations appear to be basically different.

3. The three-dimensional power spectrums of velocity and temperature fluctuations on the jet axis seem to be roughly alike - if the assumption of isotropy in this region be true. It may then follow that the difference in the one-dimensional power spectrums is a direct manifestation of the fact that velocity and heat are vector and scalar quantities, respectively.

4. The ratio of longitudinal to lateral scale (for both velocity and temperature fluctuations) is considerably larger than would follow from isotropy. Longitudinal scales are measured on the jet axis, while lateral scales involve a traverse of most of the fully turbulent core of the jet.

5. The ratio of longitudinal to lateral kinematic microscale on the jet axis is about equal to the isotropic value.

6. The longitudinal thermal microscale (from one-dimensional power spectrums) is less than the longitudinal kinematic microscale, but the lateral microscales (from correlation measurements) have the opposite relation; that is, the thermal is greater than the kinematic.

7. The probability density of the radial fluctuation $v(t)$ on the jet axis is effectively Gaussian. The probability density in the shear region is slightly skew.

8. The temperature-fluctuation field in the wake behind a local heat source consists of a randomly waving narrow laminar thermal wake. Hence the temperature signal at a fixed point is a random-pulse type of function. Its fluctuation intensity is on the order of 100 percent on the center line, and increases toward the edges.

The Johns Hopkins University
Baltimore, Md., August 17, 1949

APPENDIX A

HEAT LOSS FROM A WIRE AT VARIOUS AMBIENT TEMPERATURES

In figure 3 of reference 19 a rough check was made on the temperature-variation first term in King's (reference 27) equation for the steady static heat loss from a cylinder perpendicular to a fluid stream, at low Reynolds numbers. The conventional form is

$$\frac{i^2 R}{R - R_a} = A + B \sqrt{U} \quad (A1)$$

where

$$A = c_1 \frac{l^* k^*}{R_0 \alpha^*}$$

$$B = c_2 \frac{l^*}{R_0 \alpha^*} \sqrt{d^* c_p \rho k^*}$$

and

| | |
|---------------------------------|---|
| R | wire resistance |
| R _a | wire resistance at ambient fluid temperature |
| R ₀ | wire resistance at 0° C |
| l* | wire length |
| d* | wire diameter |
| α* | temperature coefficient of change of resistivity of wire material |
| k* | thermal conductivity of fluid at ambient temperature |
| c _p | specific heat of fluid at ambient temperature |
| ρ | density of fluid at ambient temperature |
| i | current |
| c ₁ , c ₂ | empirical constants |

In reference 19 the check on A as a function of temperature was made by assuming the second term in equation (A1) to be exact in its temperature variation. Then each measured calibration point at any velocity and temperature led to a value for A .

The present check was carried out more completely; a full calibration curve was run for each ambient temperature. From this, both A and B were determined. Figure 36 gives the results compared with King's predicted variation, using physical constants from reference 28. Each point corresponds to a calibration. The vertical line through a point obviously does not represent the over-all uncertainty; it simply shows the range of values that could be gotten by drawing different reasonable-looking straight lines through the same set of original calibration points. From the figure it can be seen that King's equation predicts the temperature variation of A quite well. The changes in B (the slope of the calibration line in the plot of $\frac{i^2 R}{R - R_a}$ against \sqrt{U}) are so small that the experimental scatter is as great as the changes predicted for these temperature differences.

APPENDIX B

MEASUREMENT OF SHEAR-CORRELATION SPECTRUM

The two voltage signals from an ideal symmetrical X-meter are

$$\left. \begin{aligned} e_1 &= \alpha u + \beta v \\ e_2 &= \alpha u - \beta v \end{aligned} \right\} \quad (B1)$$

Suppose that the velocity fluctuations are periodic:

$$\left. \begin{aligned} u &= \sum_{n=1}^{\infty} a_n \cos (2\pi n t + \phi_n) \\ v &= \sum_{n=1}^{\infty} b_n \cos (2\pi n t + \psi_n) \end{aligned} \right\} \quad (B2)$$

Of course, there would be no loss in generality if ϕ_n or ψ_n were taken as zero.

The quantity to be measured is

$${}_n R_{uv} = \frac{\overline{u_n v_n}}{\overline{u_n} \overline{v_n}} \quad (B3)$$

For two simple harmonic functions the correlation coefficient is simply the phase angle. Thus,

$${}_n R_{uv} = \cos (\phi_n - \psi_n) \quad (B4)$$

Substitution of equations (B2) into equations (B1), followed by trigonometric transformation, gives

$$\begin{aligned} e_1 &= \sum_1^{\infty} \left[(\alpha a_n \cos \phi_n + \beta b_n \cos \psi_n) \cos 2\pi n t - \right. \\ &\quad \left. (\alpha a_n \sin \phi_n + \beta b_n \sin \psi_n) \sin 2\pi n t \right] \end{aligned} \quad (B5a)$$

$$e_2 = \sum_1^{\infty} \left[(\alpha a_n \cos \phi_n - \beta b_n \cos \psi_n) \cos 2\pi n t - \right. \\ \left. (\alpha a_n \sin \phi_n - \beta b_n \sin \psi_n) \sin 2\pi n t \right] \quad (B5b)$$

When these two signals are put separately through a narrow band-pass filter that passes only the n th harmonic, the two output voltages may be represented as

$$e_{1n} = K \left[(\alpha a_n \cos \phi_n + \beta b_n \cos \psi_n) \cos 2\pi n t - \right. \\ \left. (\alpha a_n \sin \phi_n + \beta b_n \sin \psi_n) \sin 2\pi n t \right] \quad (B6a)$$

$$e_{2n} = K \left[(\alpha a_n \cos \phi_n - \beta b_n \cos \psi_n) \cos 2\pi n t - \right. \\ \left. (\alpha a_n \sin \phi_n - \beta b_n \sin \psi_n) \sin 2\pi n t \right] \quad (B6b)$$

where K is an attenuation factor.

For brevity, write

$$e_{1n} = K(A_n \cos 2\pi n t - B_n \sin 2\pi n t) \quad (B6c)$$

$$e_{2n} = K(C_n \cos 2\pi n t - D_n \sin 2\pi n t) \quad (B6d)$$

These filtered signals go next into the vacuum-thermocouple unit, which puts out the mean-square values,

$$\frac{1}{K^2} \overline{e_{1n}^2} = A_n^2 \overline{\cos^2(2\pi n t)} - 2A_n B_n \overline{\cos(2\pi n t) \sin(2\pi n t)} + \\ B_n^2 \overline{\sin^2(2\pi n t)}$$

$$\frac{1}{K'} \overline{ne_2^2} = C_n^2 \overline{\cos^2(2\pi nt)} - 2C_n D_n \overline{\cos(2\pi nt) \sin(2\pi nt)} + D_n^2 \overline{\sin^2(2\pi nt)}$$

where K' is an over-all attenuation factor.

But, $\overline{\cos^2} \approx \overline{\sin^2} \approx \frac{1}{2}$, and $\overline{\cos \sin} \approx 0$, over a large number of wavelengths. Thus,

$$\left. \begin{aligned} \overline{ne_1^2} &\approx \frac{K'}{2} (A_n^2 + B_n^2) \\ \overline{ne_2^2} &\approx \frac{K'}{2} (C_n^2 + D_n^2) \end{aligned} \right\} \quad (B7)$$

Then, within the approximation,

$$\overline{ne_1^2} - \overline{ne_2^2} = \frac{K'}{2} (A_n^2 - C_n^2 + B_n^2 - D_n^2) \quad (B8)$$

and when the expressions for A , B , C , and D are substituted, it turns out that

$$\overline{ne_1^2} - \overline{ne_2^2} = 2K'\alpha\beta a_n b_n \cos(\phi_n - \psi_n) \quad (B9)$$

The necessity of determining α and β is ordinarily avoided with a symmetrical meter, if only the correlation coefficient is required.

The sum and difference of the two wire voltages are

$$\left. \begin{aligned} e_1 + e_2 &= 2\alpha u = 2\alpha \sum_1^{\infty} a_n \cos(2\pi nt + \phi_n) \\ e_1 - e_2 &= 2\beta v = 2\beta \sum_1^{\infty} b_n \cos(2\pi nt + \psi_n) \end{aligned} \right\} \quad (B10)$$

Filtering gives

$${}_n(e_1 + e_2) = 2K\alpha a_n \cos(2\pi nt + \phi_n)$$

$${}_n(e_1 - e_2) = 2K\beta b_n \cos(2\pi nt + \psi_n)$$

Passage through the vacuum thermocouple gives

$$\left. \begin{aligned} \overline{{}_n(e_1 + e_2)^2} &= 2K'\alpha^2 a_n^2 \\ \overline{{}_n(e_1 - e_2)^2} &= 2K'\beta^2 b_n^2 \end{aligned} \right\} \quad (B11)$$

Combination of equations (B11), (B9), and (B4) gives the final result:

$${}_n R_{uv} = \frac{\overline{{}_n e_1^2} - \overline{{}_n e_2^2}}{\left[\overline{{}_n(e_1 + e_2)^2} \overline{{}_n(e_1 - e_2)^2} \right]^{1/2}} \quad (B12)$$

The computation of total-shear correlation coefficient from shear-coefficient spectrum suggests itself as a useful check possibility:

$$R_{uv} = \overline{uv} / \overline{u'^2 v'^2} \quad (B13)$$

with the Fourier series for u and v ,

$$\left. \begin{aligned} \overline{u'^2} &\equiv \overline{u^2} = \frac{1}{2} \sum_1^{\infty} a_n^2 \\ \overline{v'^2} &\equiv \overline{v^2} = \frac{1}{2} \sum_1^{\infty} b_n^2 \end{aligned} \right\} \quad (B14)$$

and the instantaneous cross product can be transformed to

$$uv = \sum_{n=1}^{\infty} \sum_{m=1}^{\infty} a_n b_m (\cos \phi_n \cos 2\pi n t - \sin \phi_n \sin 2\pi n t) \times \\ (\cos \psi_m \cos 2\pi m t - \sin \psi_m \sin 2\pi m t)$$

The time average of this expression is

$$\overline{uv} = \frac{1}{2} \sum_{n=1}^{\infty} a_n b_n (\cos \phi_n \cos \psi_n + \sin \phi_n \sin \psi_n)$$

or

$$\overline{uv} = \frac{1}{2} \sum_{n=1}^{\infty} a_n b_n \cos (\phi_n - \psi_n) \quad (B15)$$

Thus,

$$u'v' R_{uv} = \frac{1}{2} \sum_{n=1}^{\infty} a_n b_n n R_{uv}$$

In terms of the Fourier coefficients,

$$R_{uv} = \frac{\sum_{n=1}^{\infty} a_n b_n n R_{uv}}{\left(\sum_{n=1}^{\infty} a_n^2 \sum_{n=1}^{\infty} b_n^2 \right)^{1/2}} \quad (B16)$$

But $n^F u \equiv a_n^2 / \sum_{n=1}^{\infty} a_n^2$ and $n^F v \equiv b_n^2 / \sum_{n=1}^{\infty} b_n^2$ are simply the normalized one-dimensional energy spectrums of u and v , respectively. Therefore,

$$R_{uv} = \sum_{n=1}^{\infty} (n^F u n^F v)^{1/2} n R_{uv} \quad (B17)$$

REFERENCES

1. Kolmogoroff, A.: The Local Structure of Turbulence in Incompressible Viscous Fluid for Very Large Reynolds' Numbers. *Comp. rend., acad. sci. URSS*, vol. 30, no. 4, Feb. 10, 1941, pp. 301-305.
2. Kolmogoroff, A. N.: Dissipation of Energy in the Locally Isotropic Turbulence. *Comp. rend., acad. sci. URSS*, vol. 32, no. 1, July 10, 1941, pp. 16-18.
3. Townsend, A. A.: Measurements in the Turbulent Wake of a Cylinder. *Proc. Roy. Soc. (London)*, ser. A, vol. 190, no. 1023, Sept. 9, 1947, pp. 551-561.
4. Townsend, A. A.: Local Isotropy in the Turbulent Wake of a Cylinder. *Australian Jour. Sci. Res.*, ser. A, vol. 1, no. 2, 1948, pp. 161-174.
5. Schubauer, G. B., and Klebanoff, P. S.: Theory and Application of Hot-Wire Instruments in the Investigation of Turbulent Boundary Layers. NACA ACR 5K27, 1946.
6. Schubauer, G. B., and Klebanoff, P. S.: Investigation of Separation of the Turbulent Boundary Layer. NACA TN 2133, 1950.
7. Laufer, John: Investigation of Turbulent Flow in a Two-Dimensional Channel. NACA TN 2123, 1950.
8. Liepmann, Hans Wolfgang, and Laufer, John: Investigations of Free Turbulent Mixing. NACA TN 1257, 1947.
9. Corrsin, Stanley: Investigation of Flow in an Axially Symmetrical Heated Jet of Air. NACA ACR 3L23, 1943.
10. Corrsin, Stanley, and Uberoi, Mahinder S.: Further Experiments on the Flow and Heat Transfer in a Heated Turbulent Air Jet. NACA TN 1865, 1949.
11. Taylor, G. I.: Diffusion by Continuous Movements. *Proc. London Math. Soc.*, ser. A, vol. 20, 1922, pp. 196-212.
12. Schubauer, G. B.: A Turbulence Indication Utilizing the Diffusion of Heat. NACA Rep. 524, 1935.
13. Taylor, G. I.: Statistical Theory of Turbulence. IV - Diffusion in a Turbulent Air Stream. *Proc. Roy. Soc. (London)*, ser. A, vol. 151, no. 873, Sept. 2, 1935, pp. 465-478.

14. Skramstad, H. K., and Schubauer, G. B.: The Application of Thermal Diffusion to the Study of Turbulent Air Flow. Phys. Rev., vol. 53, no. 11, June 1, 1938, p. 927.
15. Dryden, Hugh L.: Turbulence and Diffusion. Ind. and Eng. Chem., vol. 31, no. 4, April 1939, pp. 416-425.
16. Wieghardt, K.: Über Ausbreitungsvorgänge in turbulenten Reibungsschichten. Z.f.a.M.M., Bd. 28, Heft 11/12, Nov./Dec. 1948, pp. 346-355.
17. Kovasznay, L.: Calibration and Measurement in Turbulence Research by the Hot-Wire Method. NACA TM 1130, 1947.
18. Scott, H. H.: The Degenerative Sound Analyzer. Jour. Acous. Soc. Am., vol. 11, no. 2, Oct. 1939, pp. 225-232.
19. Corrsin, Stanley: Extended Applications of the Hot-Wire Anemometer. NACA TN 1864, 1949; abstract in Rev. Sci. Instr., vol. 18, no. 7, July 1947, pp. 469-471.
20. Von Kármán, Th.: Progress in the Statistical Theory of Turbulence. Proc. Nat. Acad. Sci., vol. 34, no. 11, Nov. 1948, pp. 530-539.
21. Dryden, Hugh L.: A Review of the Statistical Theory of Turbulence. Quart. Appl. Math., vol. I, no. 1, April 1943, pp. 7-42.
22. Heisenberg, W.: Zur statistischen Theorie der Turbulenz. Zeitschr. Phys., Bd. 124, Heft 7/12, 1948, pp. 628-657.
23. Kovasznay, L. S. G., Uberoi, M. S., and Corrsin, S.: The Transformation between One- and Three-Dimensional Power Spectra for an Isotropic Scalar Fluctuation Field. Phys. Rev., vol. 76, no. 8, Oct. 15, 1949, pp. 1263-1264.
24. Taylor, G. I.: Statistical Theory of Turbulence. Part I. Proc. Roy. Soc. (London), ser. A, vol. 151, no. 873, Sept. 2, 1935, pp. 423-444.
25. Corrsin, S.: Decay of Turbulence behind Three Similar Grids. A.E. Thesis, C. I. T., 1942.
26. Ruden, P.: Turbulente Ausbreitungsvorgänge im Freistrah. Die Naturwissenschaften, Jahrg. 21, Heft 21/23, May 26, 1933, pp. 375-378.

27. King, Louis Vessot: On the Convection of Heat from Small Cylinders in a Stream of Fluid: Determination of the Convection Constants of Small Platinum Wires with Applications to Hot-Wire Anemometry. Phil. Trans. Roy. Soc. (London), ser. A, vol. 214, Nov. 12, 1914, pp. 373-432.
28. Anon.: International Critical Tables. Vol. V. McGraw-Hill Book Co., Inc., 1929.

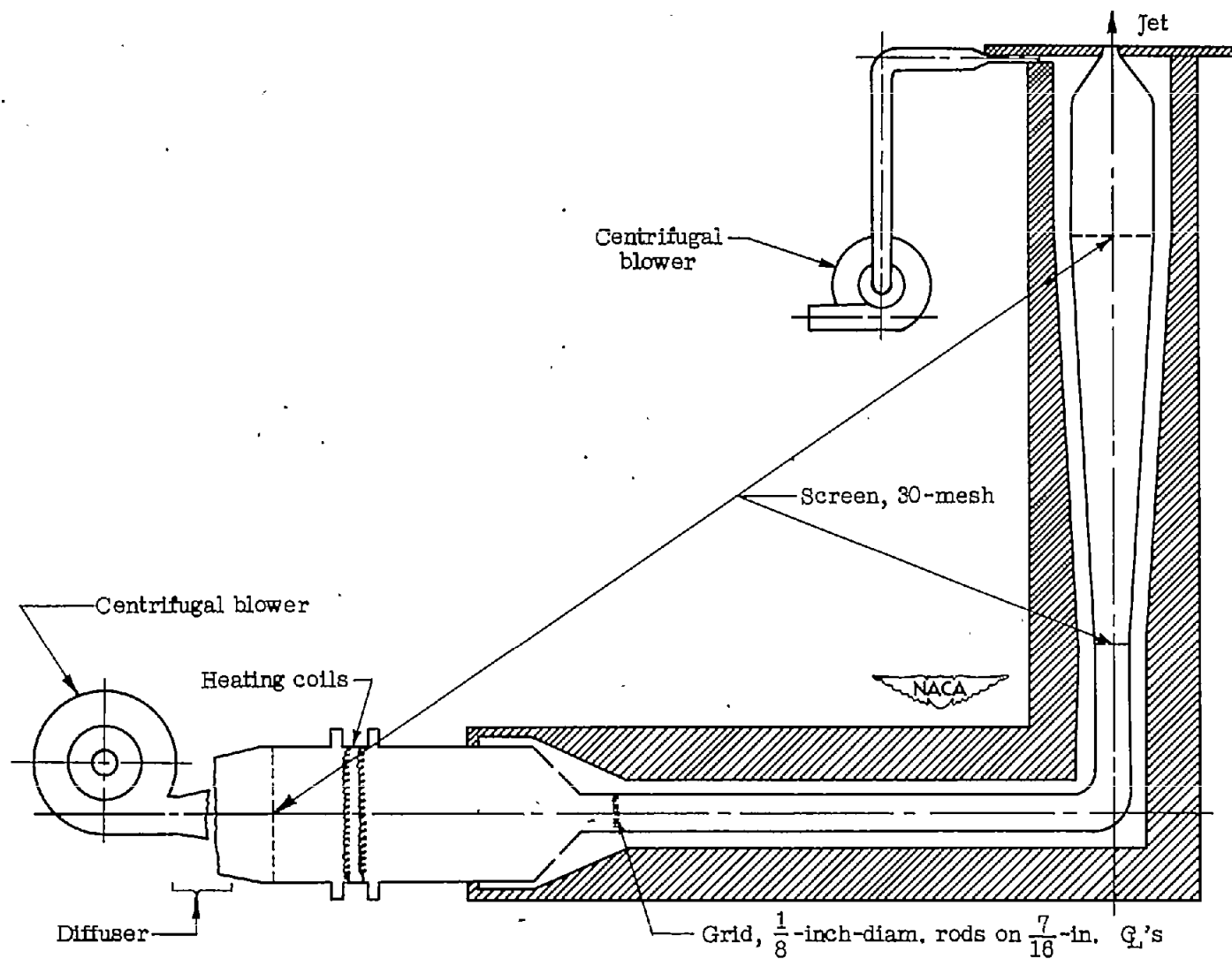


Figure 1.- Schematic diagram of 1-inch hot-jet unit.

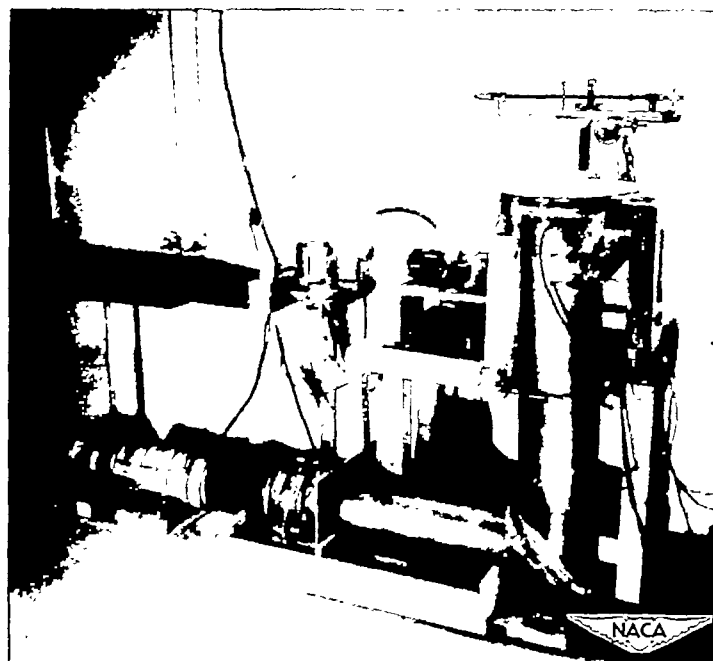


Figure 2.- The jet unit.

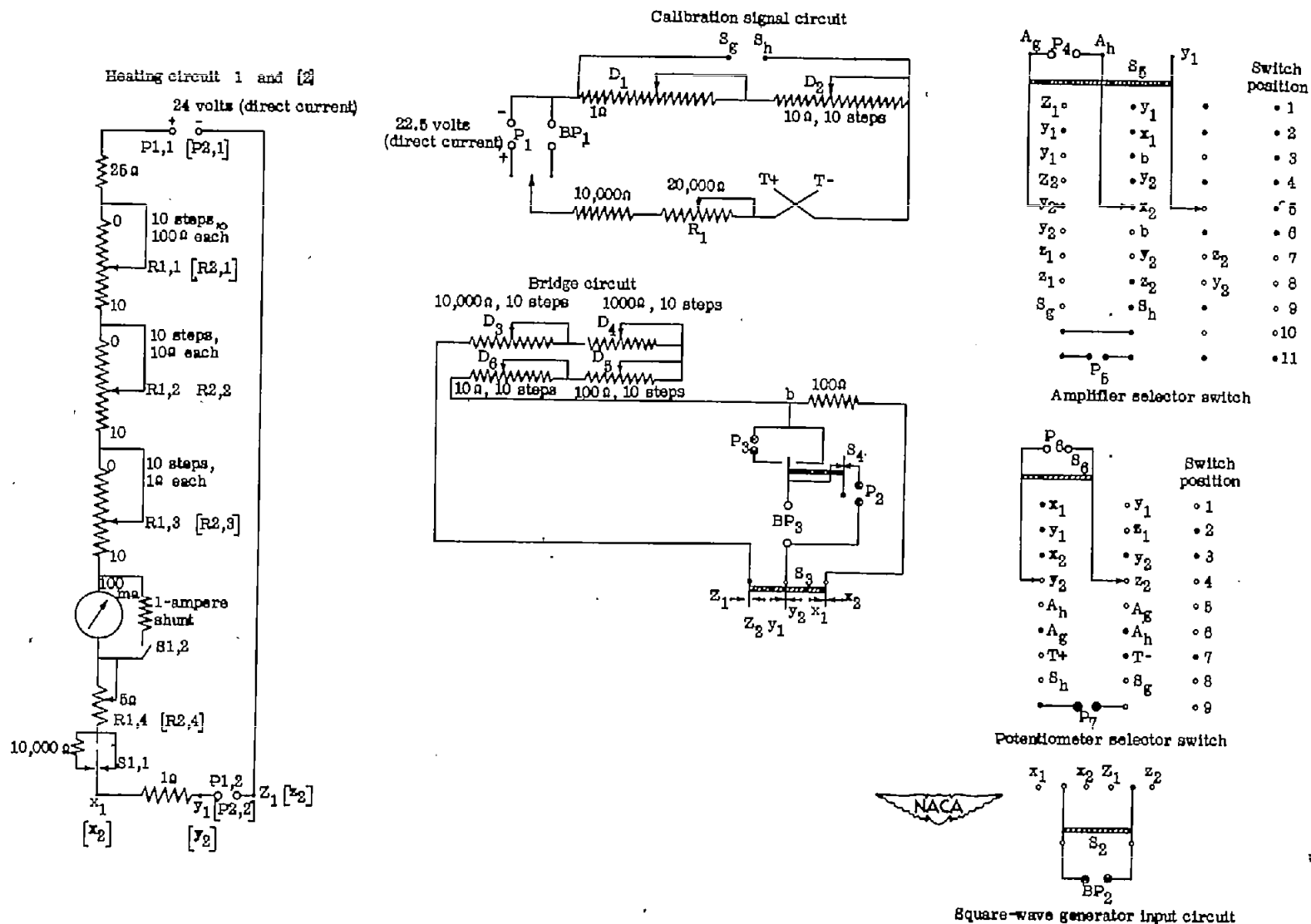


Figure 3.- Control circuits.

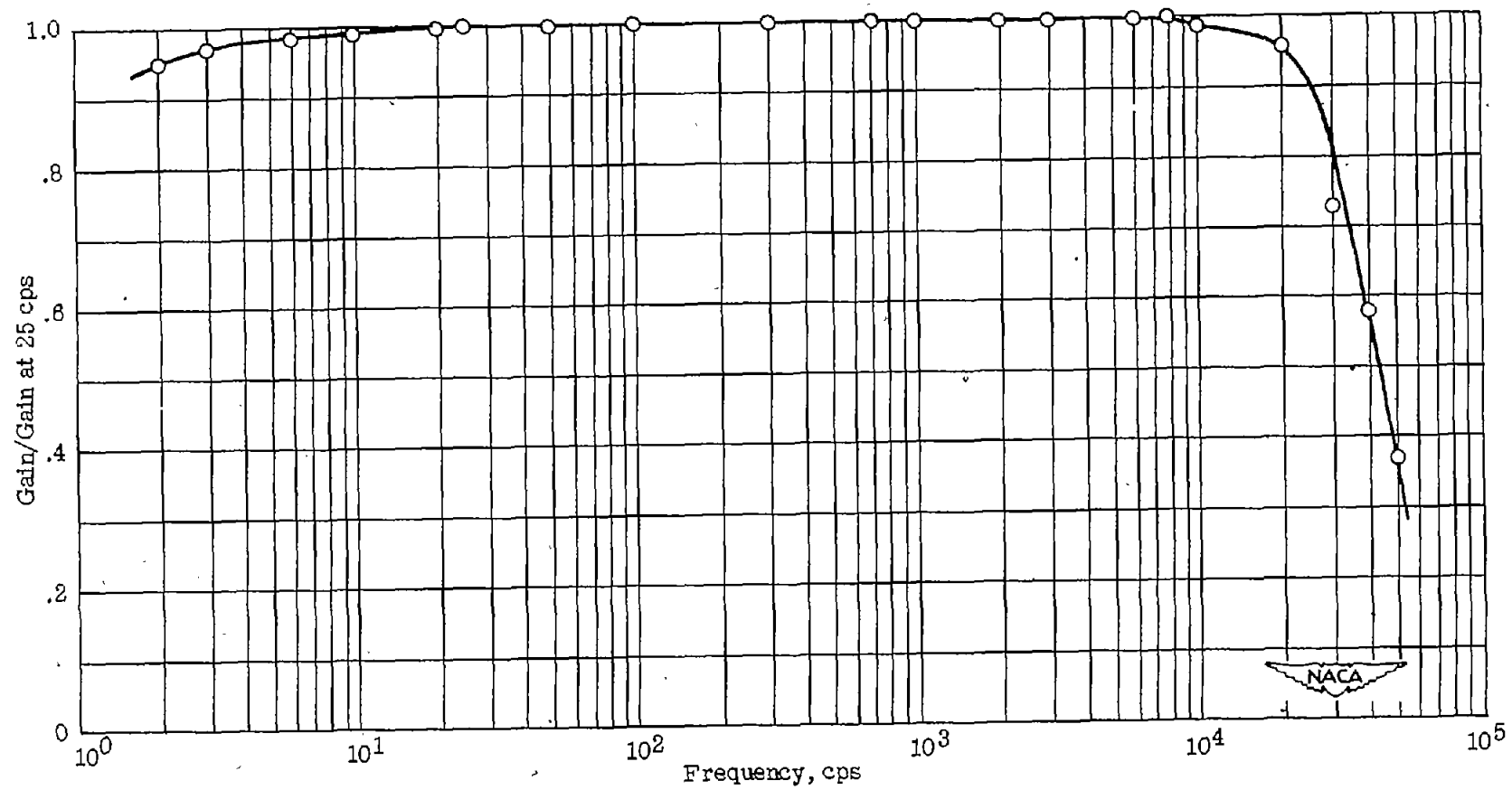
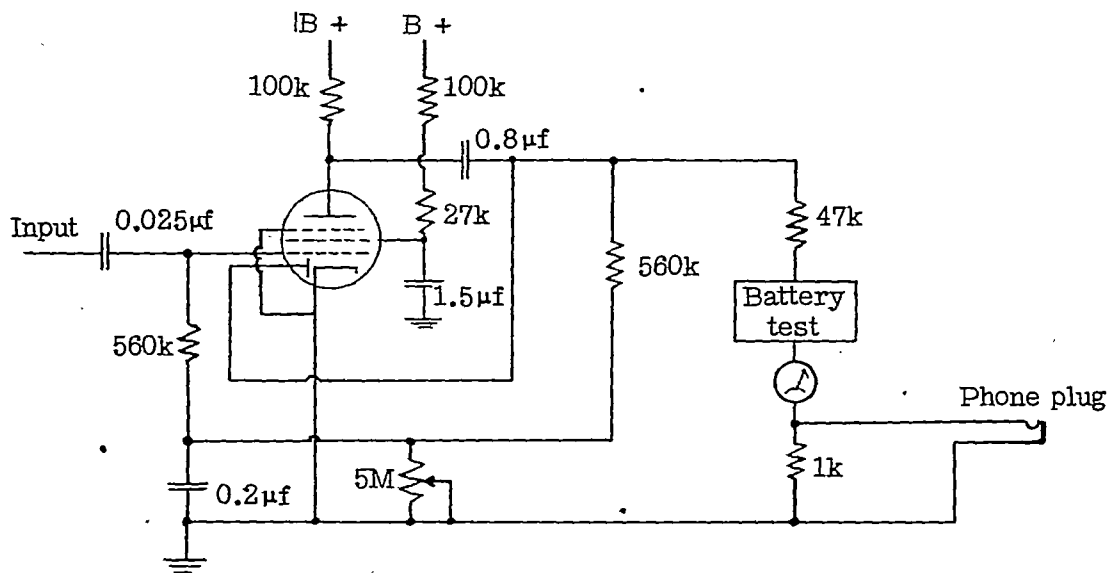
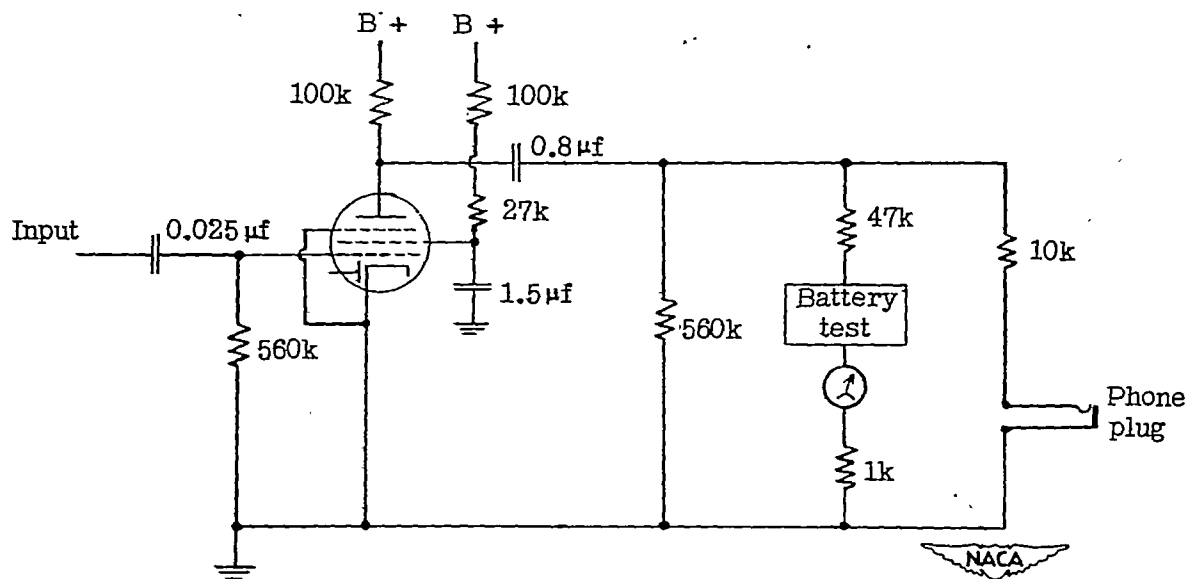


Figure 5.- Amplifier frequency response without compensation.



(a) Original output circuit.



(b) Modified output circuit.

Figure 6.- Modification of General Radio Type 760-A Sound Analyzer.

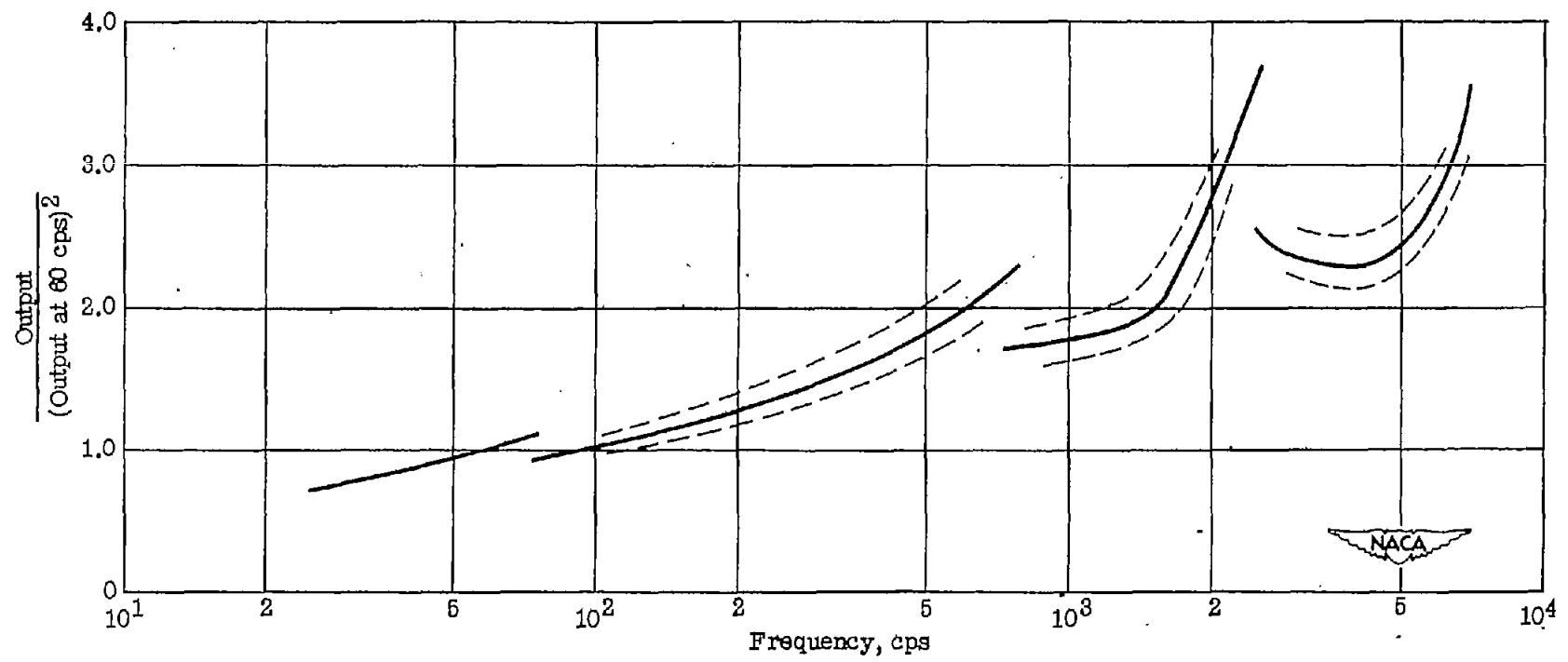


Figure 7.- Response of sound analyzer with modified output circuit.

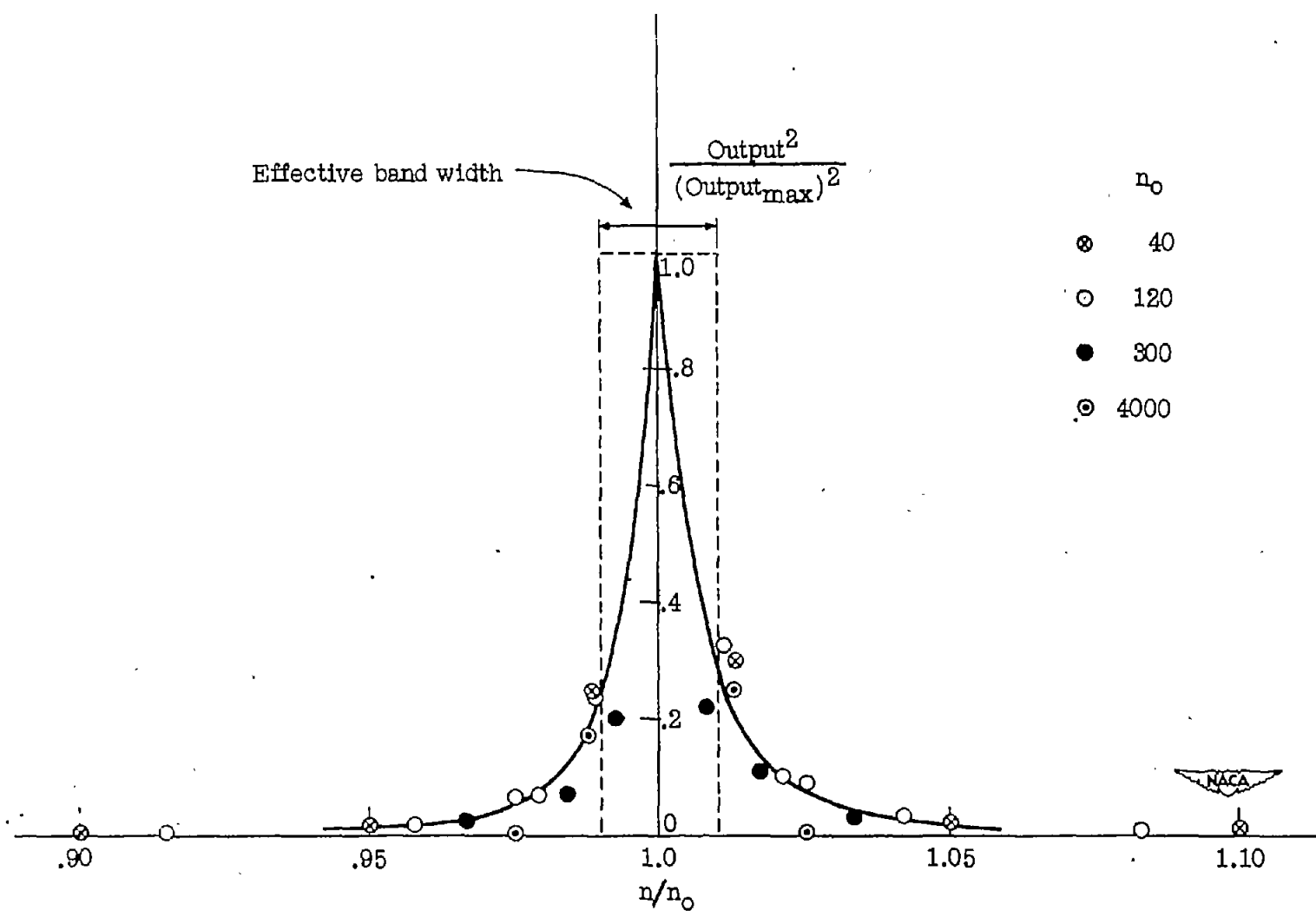


Figure 8.- Filtration characteristics of sound analyser with modified output circuit. Area of rectangle equals area under curve.

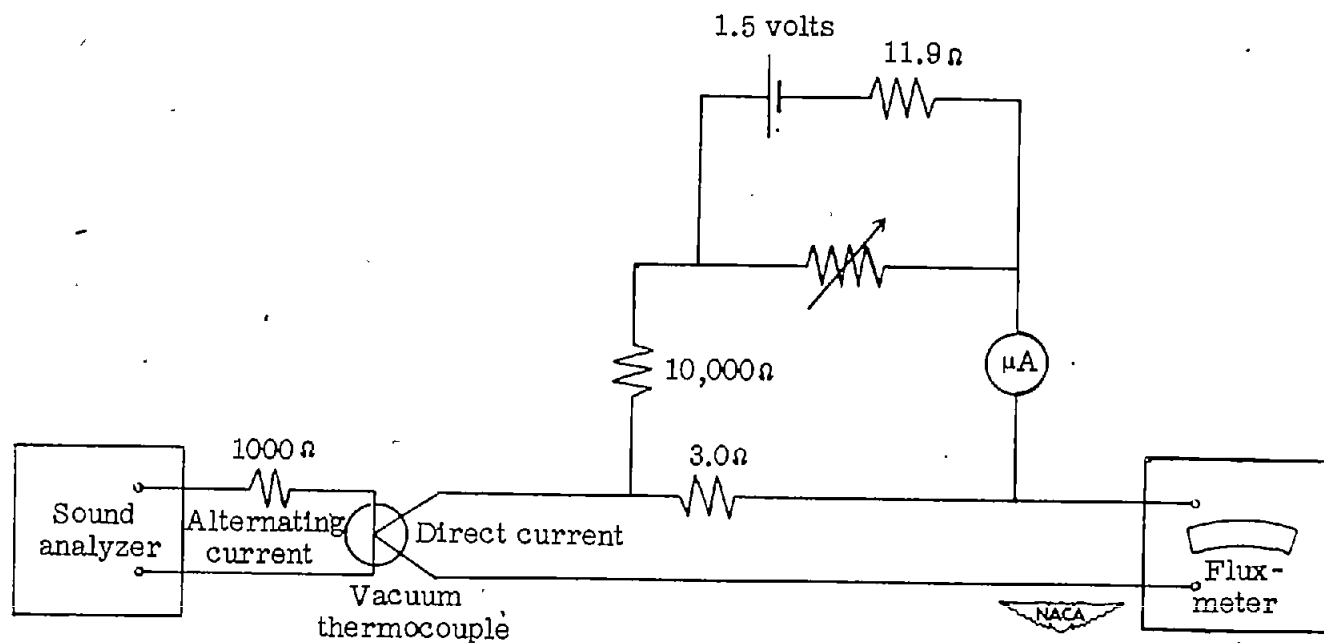


Figure 9.- Integrator and bucking circuit.

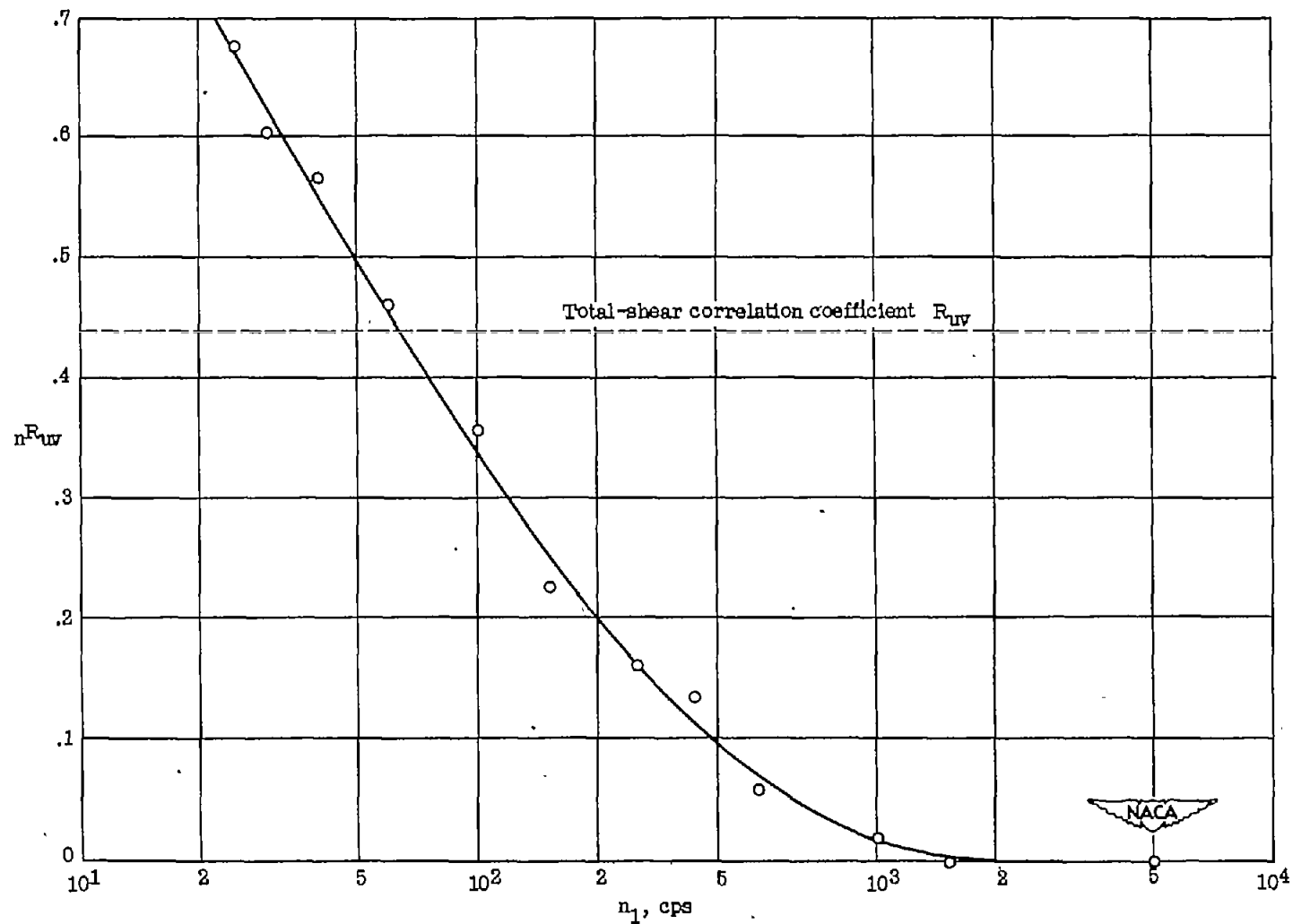


Figure 10.- Variation of shear correlation coefficient nR_{uv} with frequency. Round turbulent jet. $x/d = 20$;
 $\bar{U} = 270$ centimeters per second.

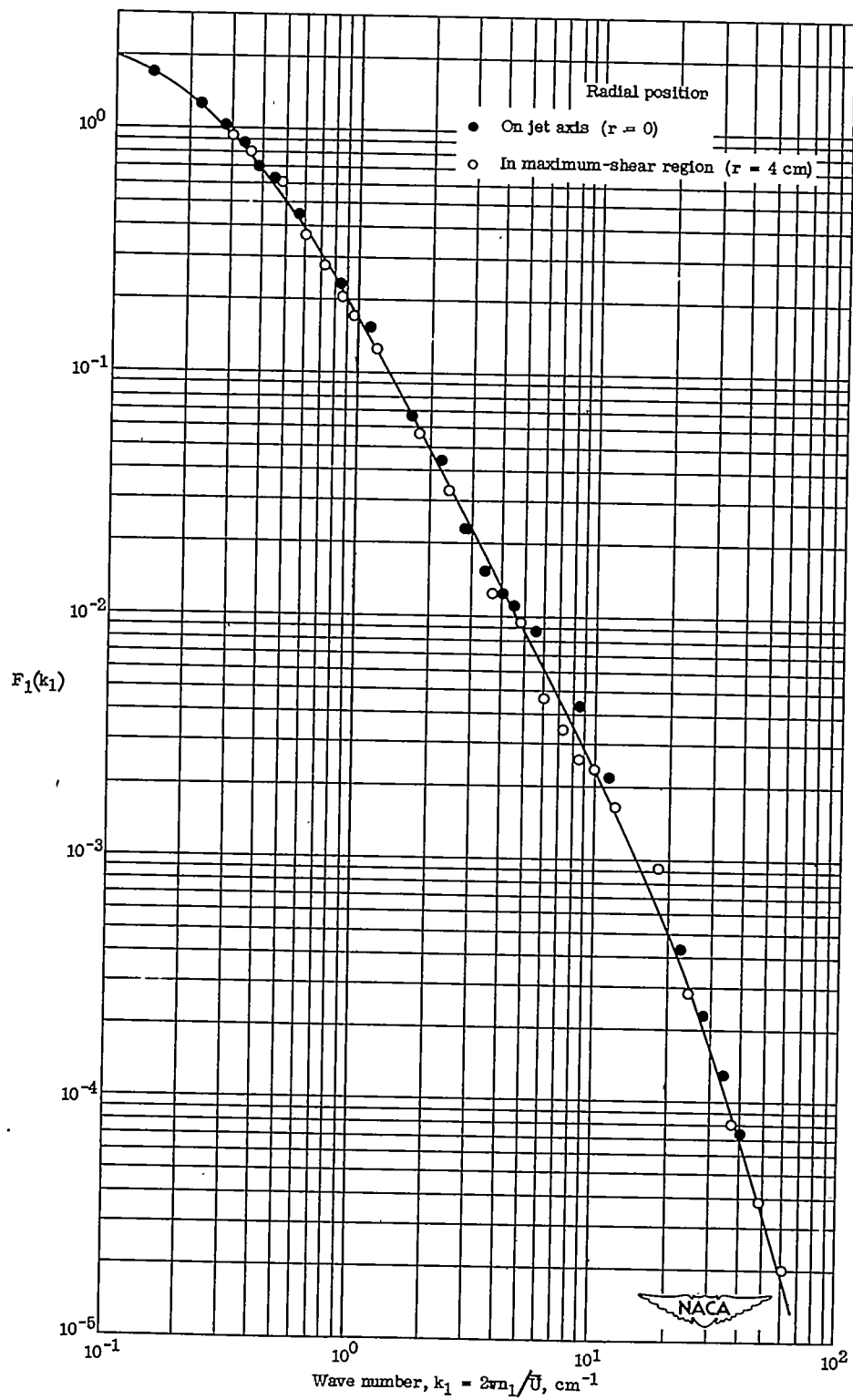


Figure 11.- One-dimensional power spectrums of $u(t)$ measured in 1-inch unheated jet at $x/d = 20$. Computed scales: $L_x = 3.3$ centimeters for both stations, $\lambda_x = 0.31$ centimeter for both stations.

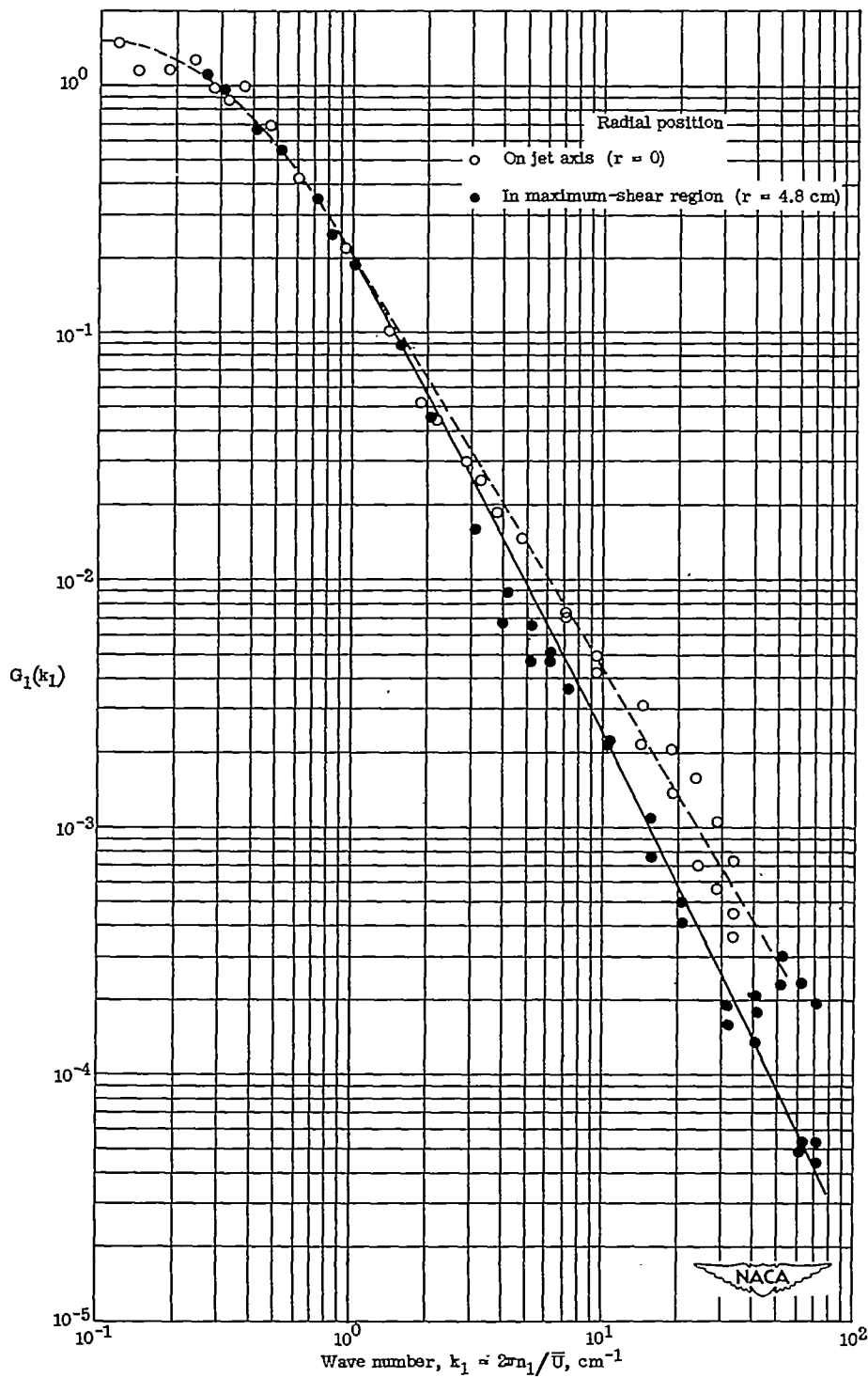


Figure 12.- One-dimensional power spectrums of $\vartheta(t)$ measured in 1-inch heated jet at $x/d = 20$. Computed scales: $\Lambda_x = \frac{\pi}{2} G_1(0) = 2.18$ centimeters for both stations.

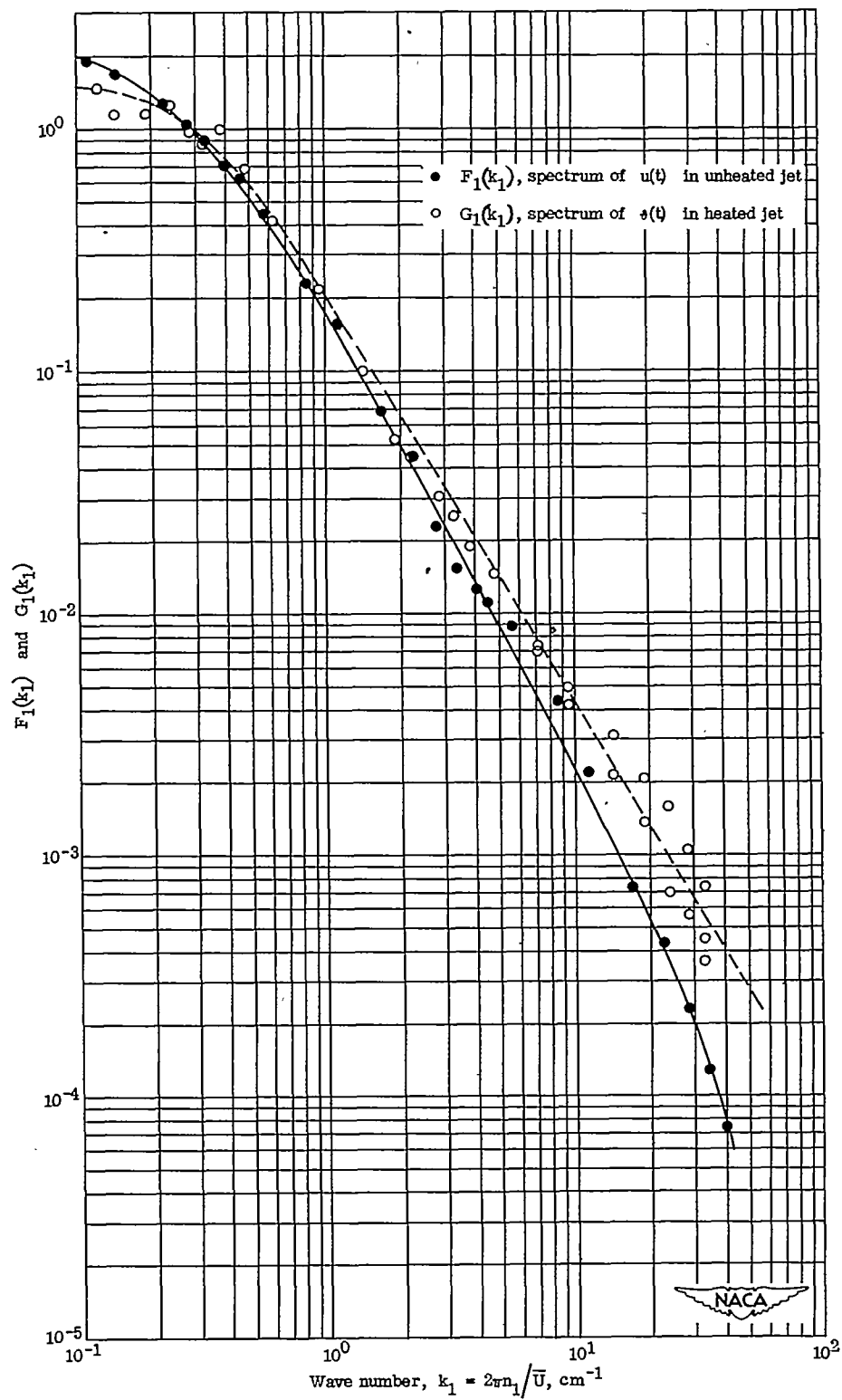


Figure 13.- One-dimensional spectrums of $u(t)$ and $\vartheta(t)$ on axis of 1-inch jet at $x/d = 20$.

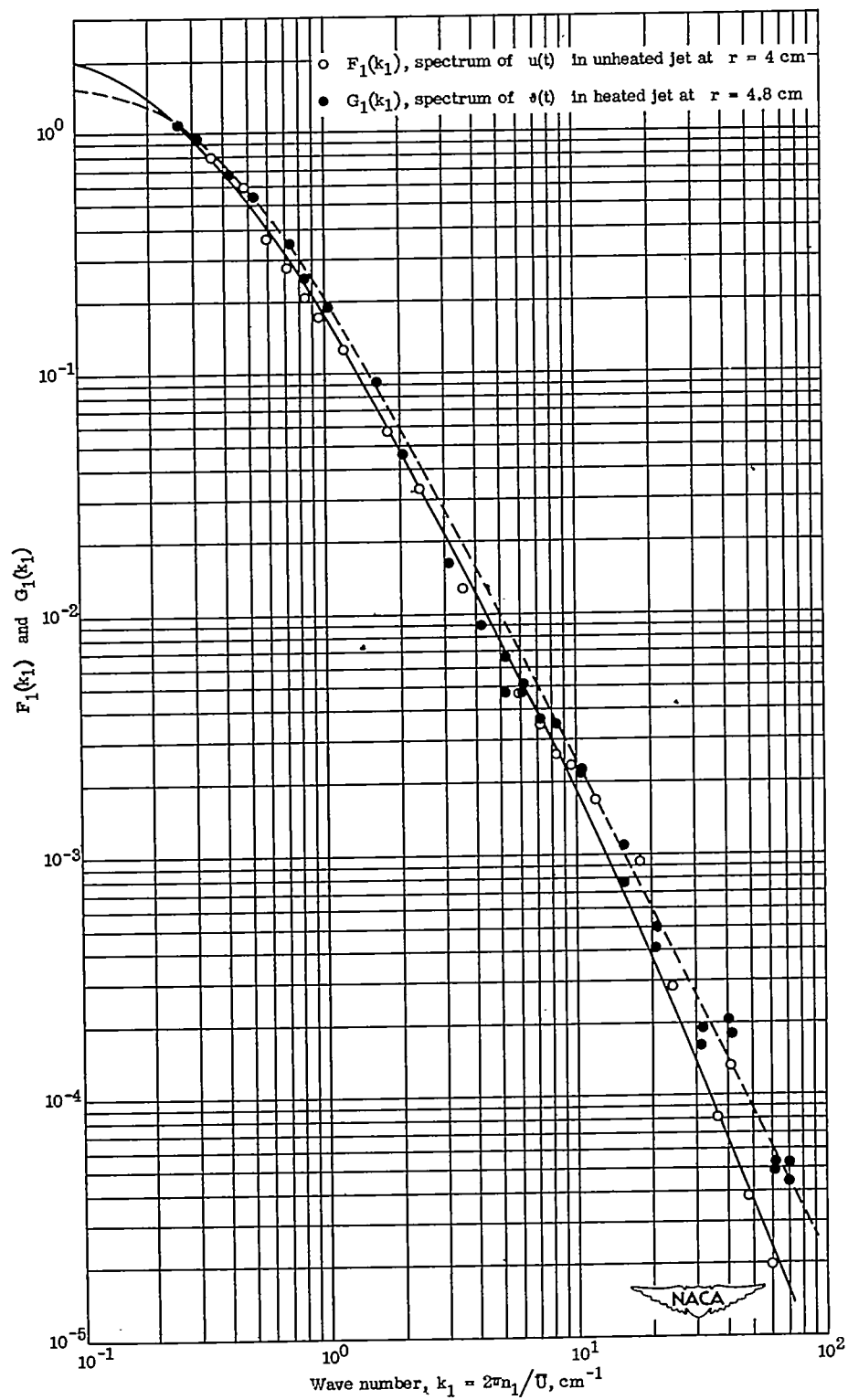


Figure 14.- One-dimensional power spectrums of $u(t)$ and $\vartheta(t)$ in maximum-shear region of 1-inch jet at $x/d = 20$.

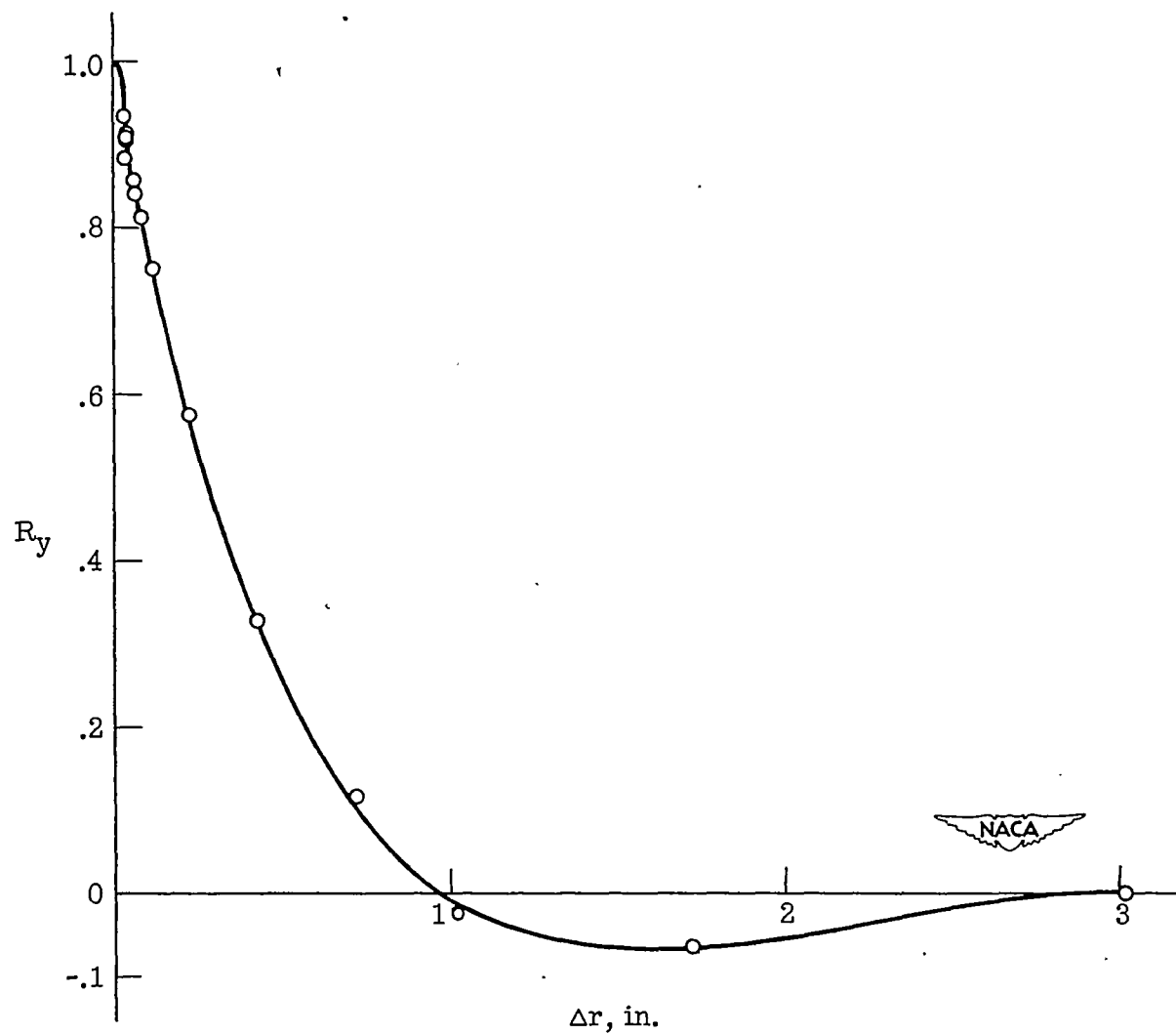


Figure 15.- Symmetric transverse correlation of u , measured about axis at $x/d = 20$ in 1-inch unheated jet. $R_y = \overline{u_1 u_2} / u^2$.

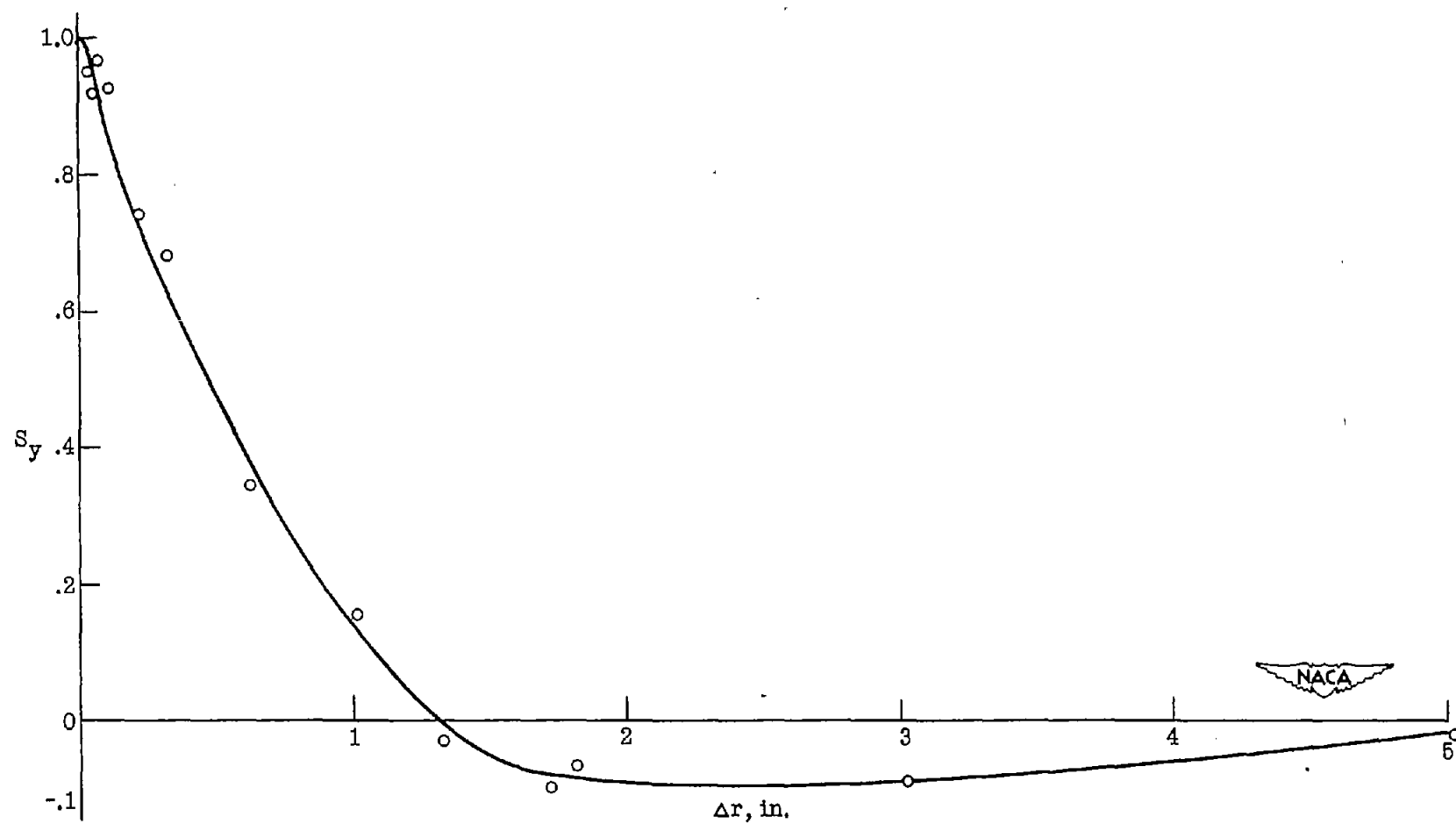


Figure 16.- Symmetric transverse correlation of ϕ , measured at $x/d = 20$ in 1-inch heated jet.

$$S_y = \overline{\phi_1 \phi_2} / \overline{\phi^2}.$$

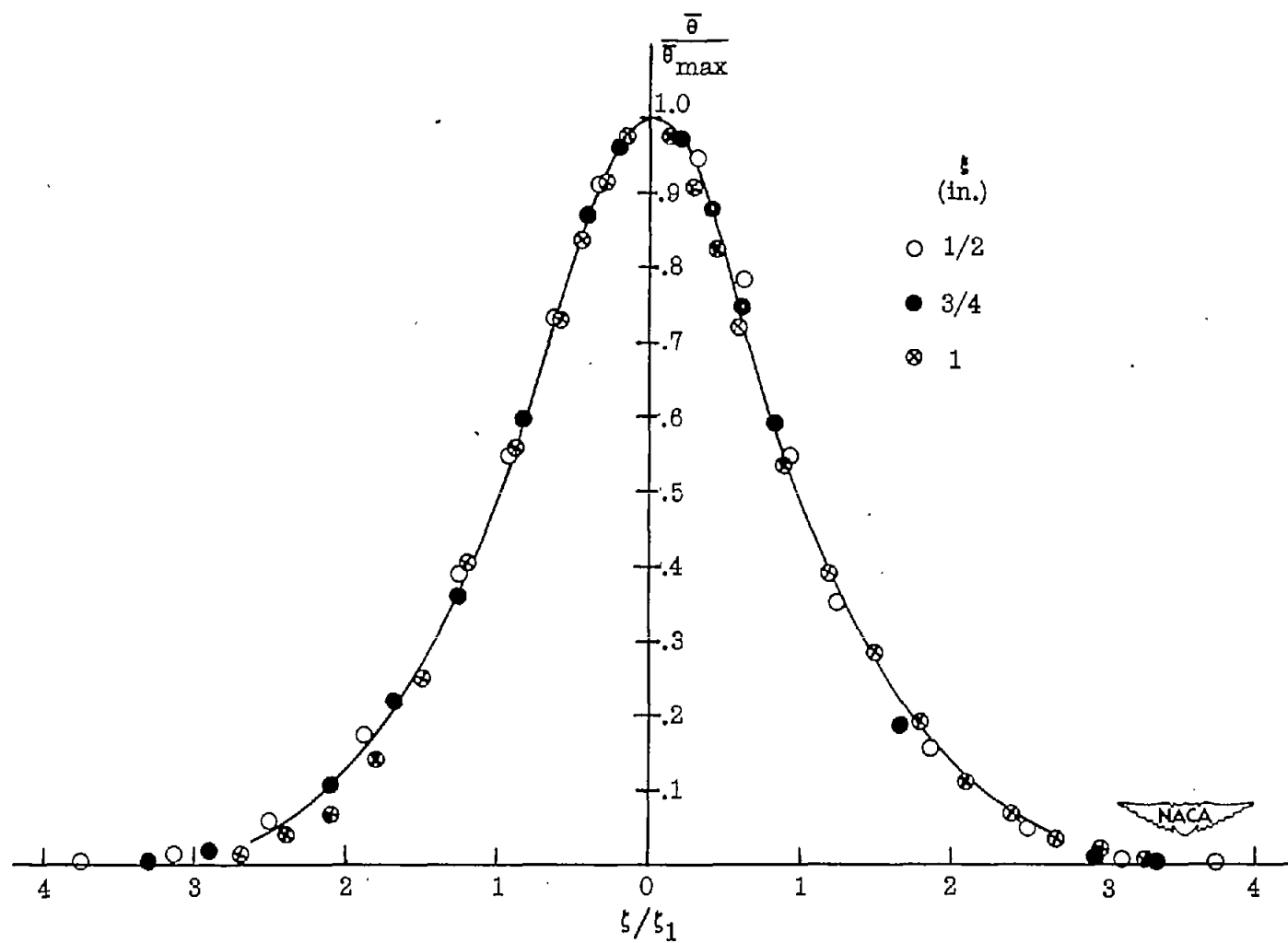


Figure 17.- Similarity of temperature behind line source of heat on jet axis at $x/d = 20$ in unheated jet.

$$\zeta_1 = \zeta \text{ at which } \bar{\theta} = \frac{1}{2} \bar{\theta}_{max}.$$

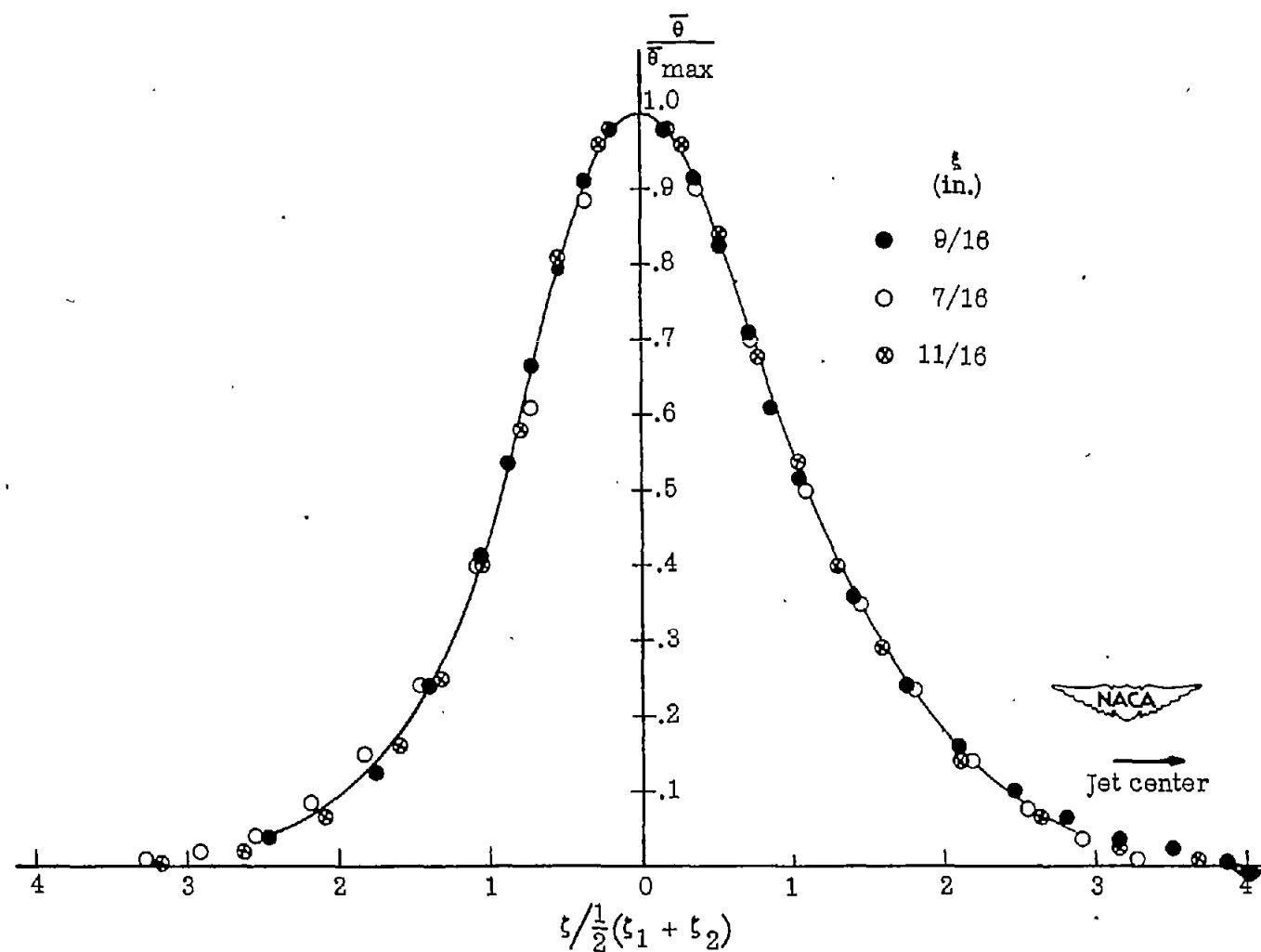


Figure 18.- Similarity of temperature distribution behind 2-inch-diameter-ring source of heat in unheated jet at $x/d = 20$. $\xi_1, \xi_2 = \xi$ at which $\bar{\theta} = \frac{1}{2}\bar{\theta}_{max}$.

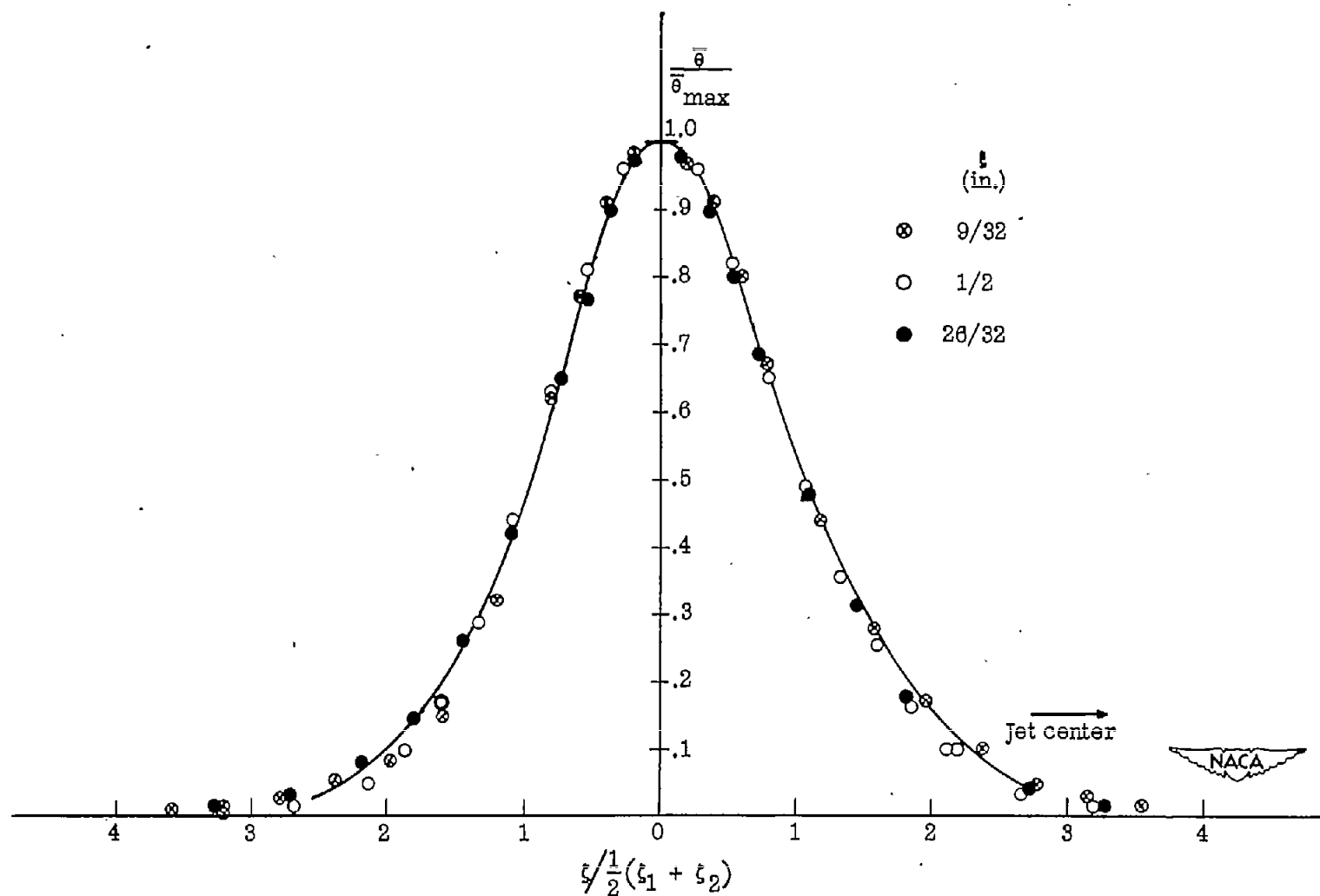


Figure 19.- Similarity of temperature behind 4-inch-diameter-ring source of heat in unheated jet at $x/d = 20$. $\xi_1, \xi_2 = \xi$ at which $\bar{\theta} = \frac{1}{2} \bar{\theta}_{max}$.

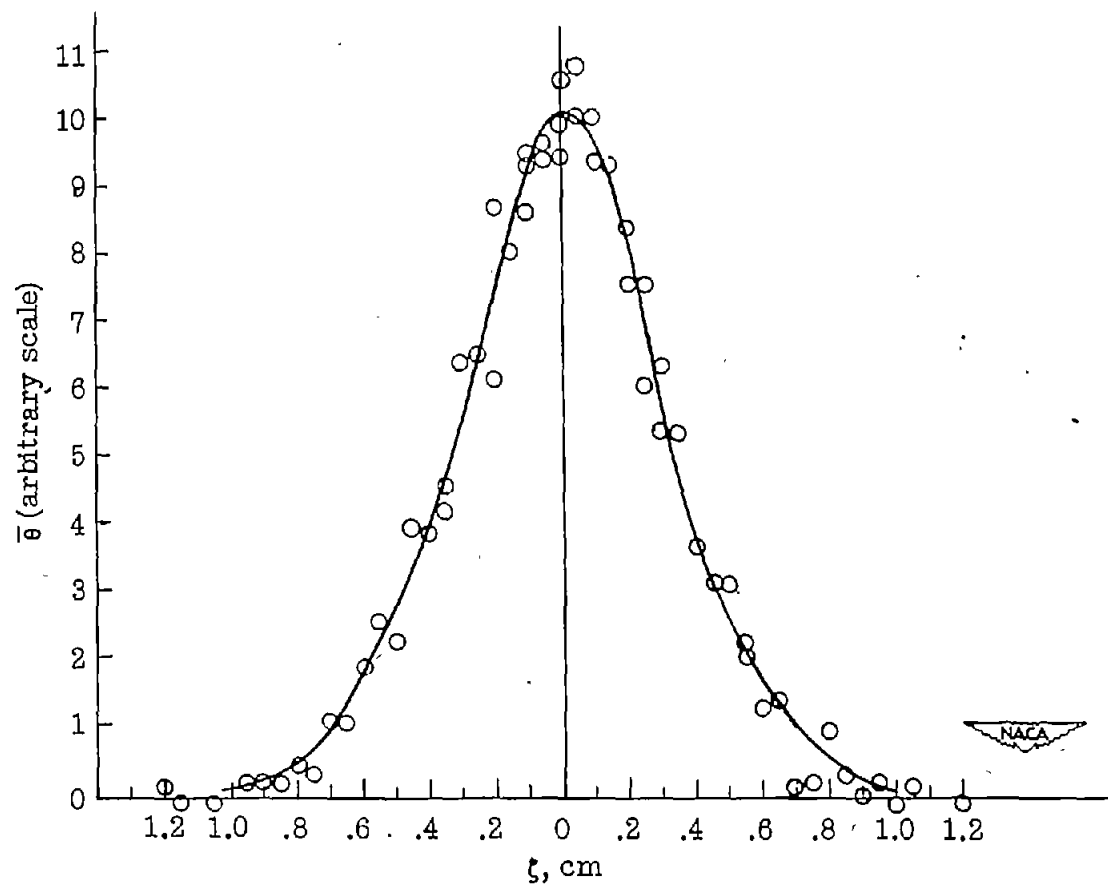


Figure 20.- Experimental scatter; temperature behind line source of heat on jet axis. $\xi = 1.27$ centimeters;
 $x/d = 20$.

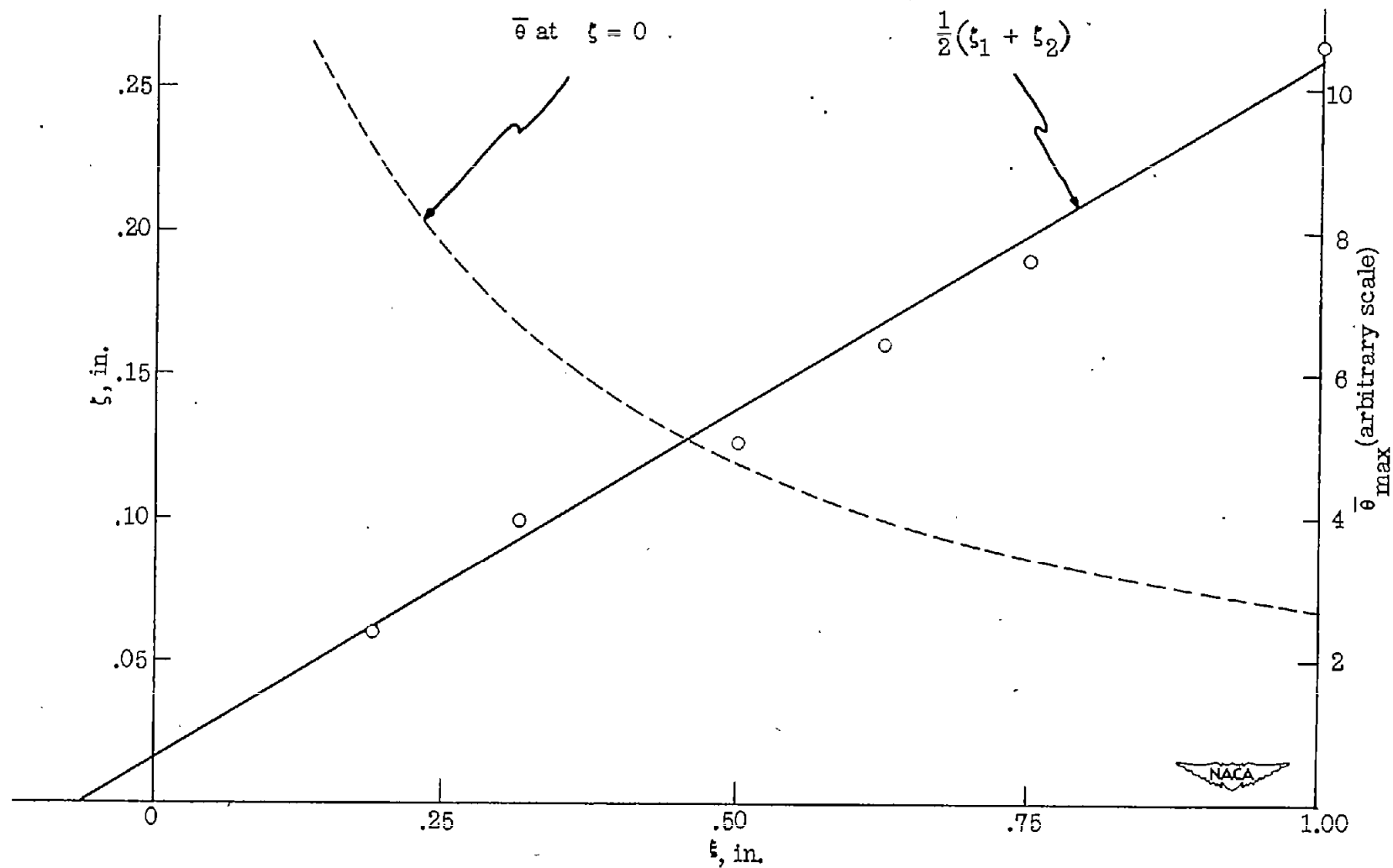


Figure 21.- Spread of heat from a line source in center of unheated jet. $x/d = 20$. $\zeta_1 = \zeta$ at which

$$\bar{\theta} = \frac{1}{2}\bar{\theta}_{\max}$$

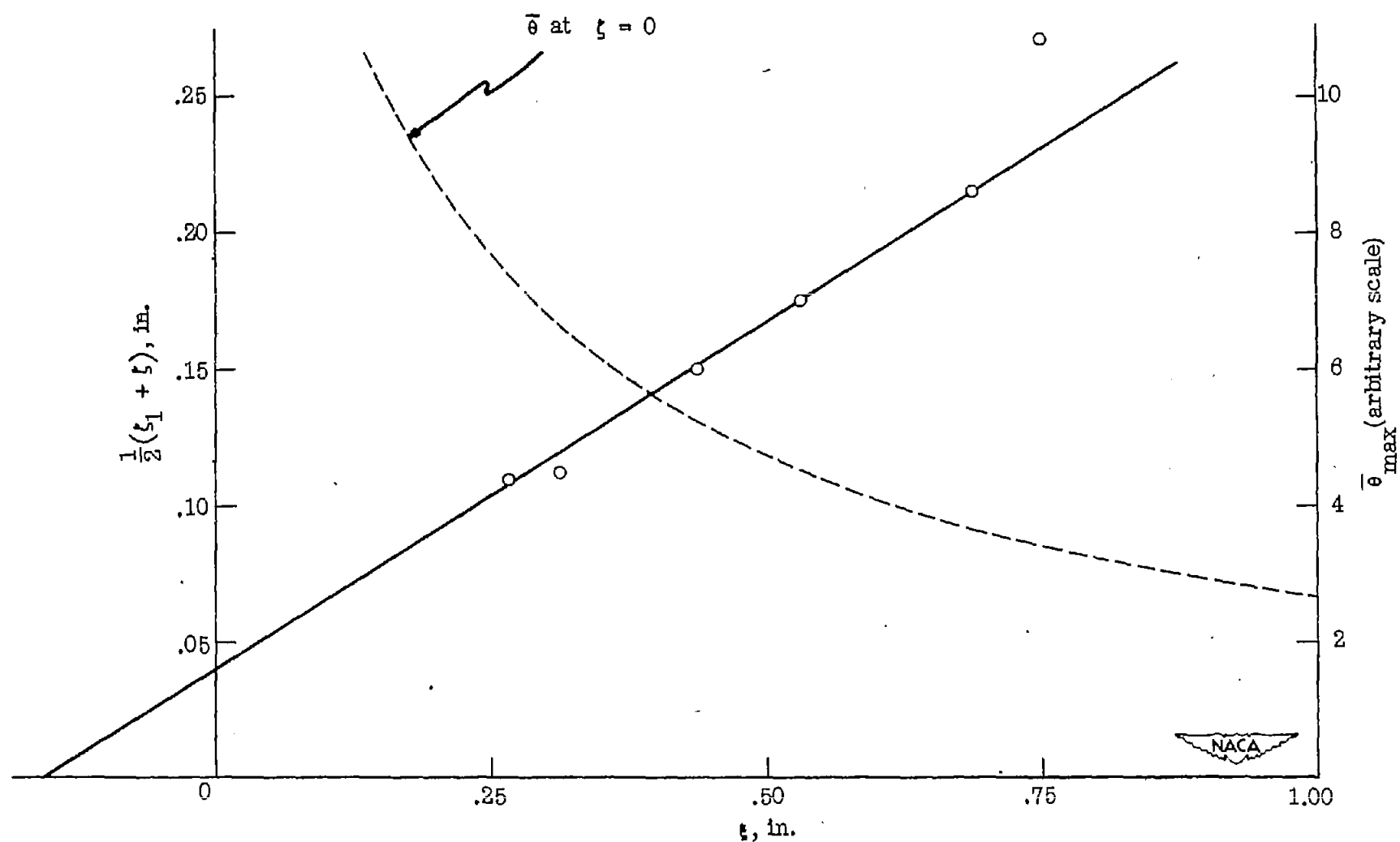


Figure 22.- Spread of heat from 2-inch-diameter-ring source in unheated jet. $x/d = 20$. $\xi_1, \xi = \xi$ at which

$$\bar{\theta} = \frac{1}{2}\bar{\theta}_{\max}.$$

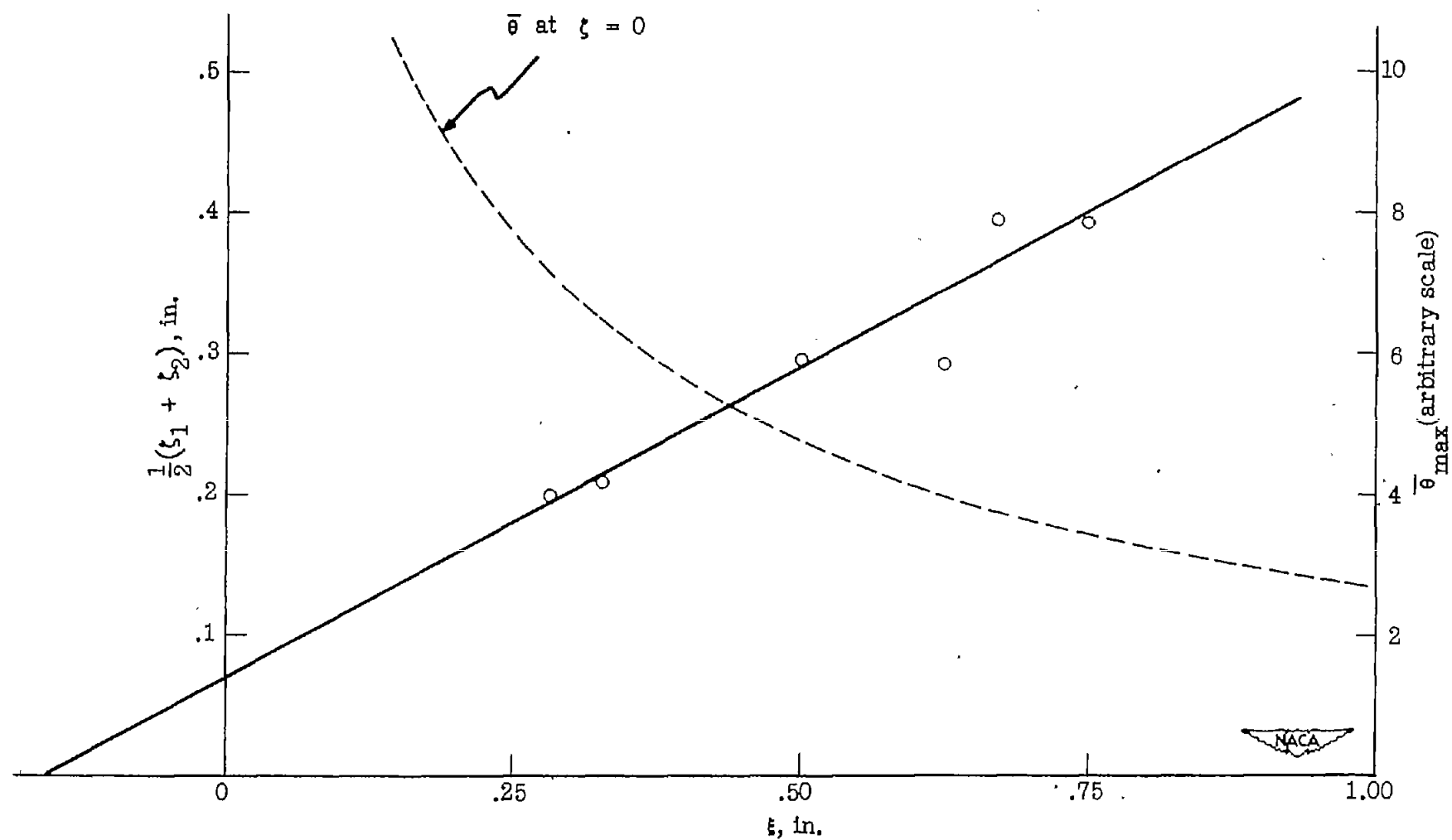


Figure 23.- Spread of heat from 4-inch-diameter-ring source in unheated jet. $x/d = 20$. $t_1, t_2 = t$ at which $\bar{\theta} = \frac{1}{2}\bar{\theta}_{\max}$.

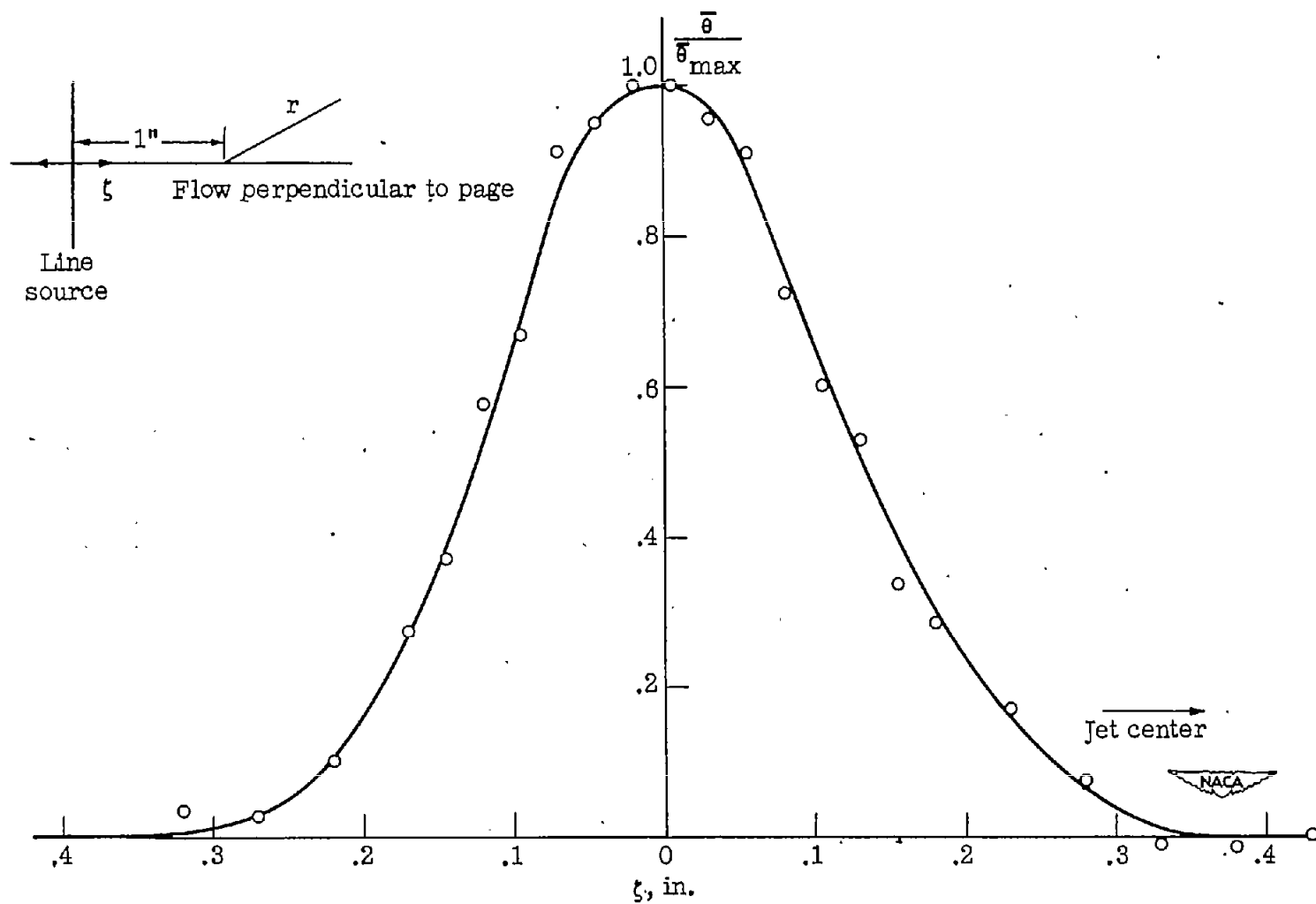


Figure 24.- Temperature behind line source of heat in unheated jet. $x/d = 20$; $\xi = 1/2$ inch. Line source set perpendicular to r at a radius of 1 inch. Traverse made in r -direction.

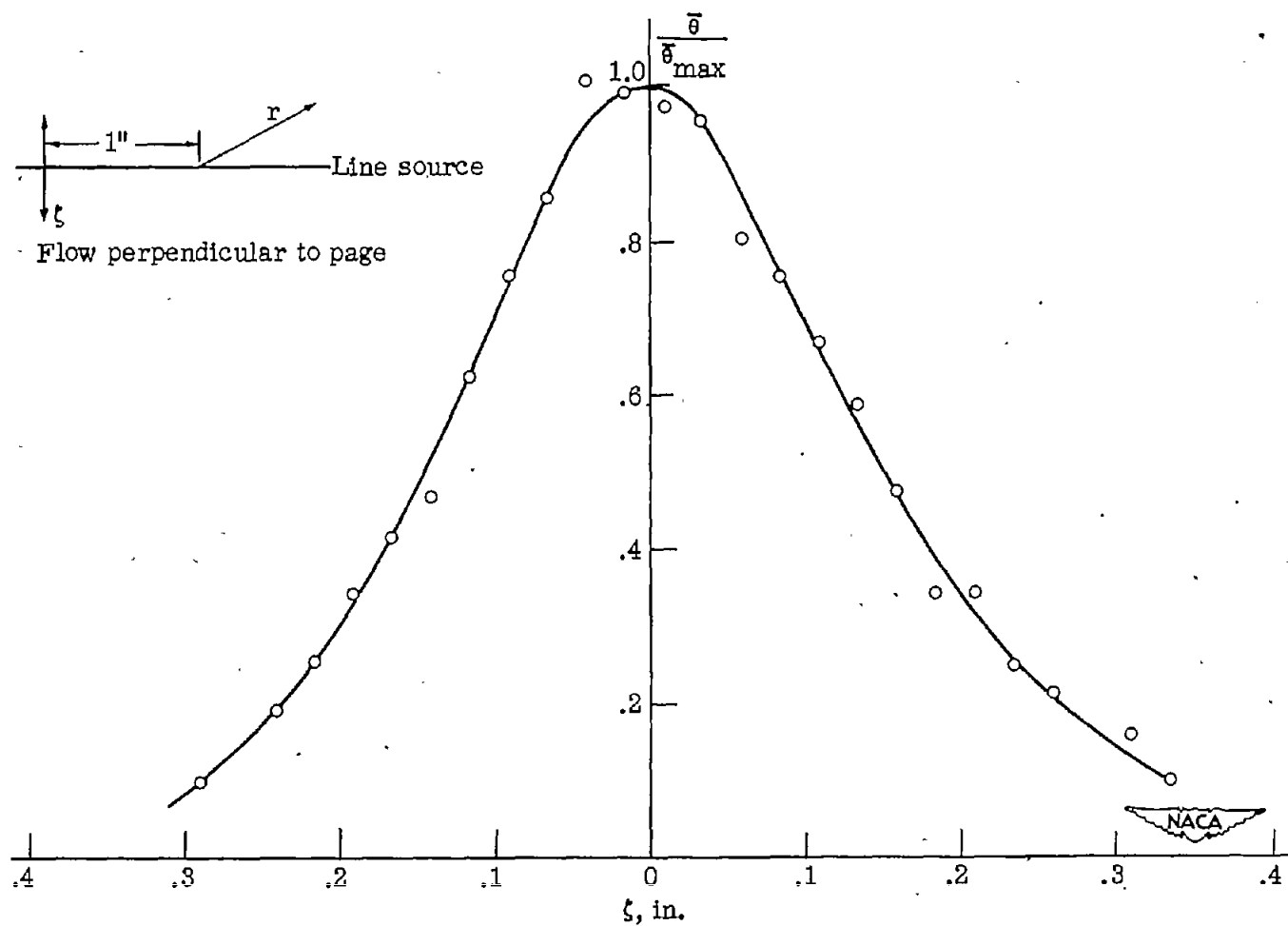


Figure 25.- Temperature behind line source of heat in unheated jet. $x/d = 20$; $z = 1/2$ inch. Line source set on a diametral line. Traverse made perpendicular to r at a radius of 1 inch.

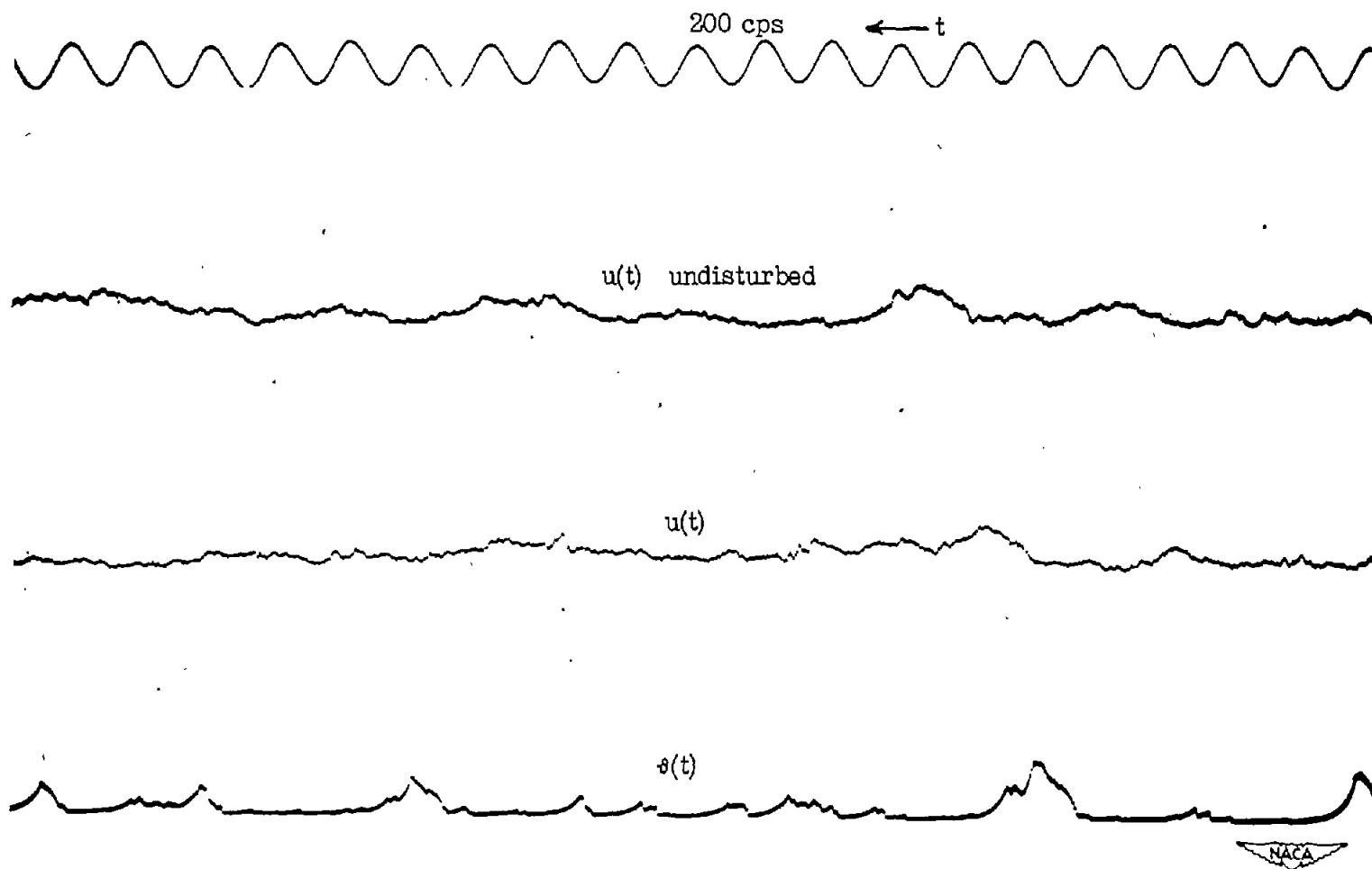


Figure 28.- Oscillograms of velocity and temperature fluctuations.

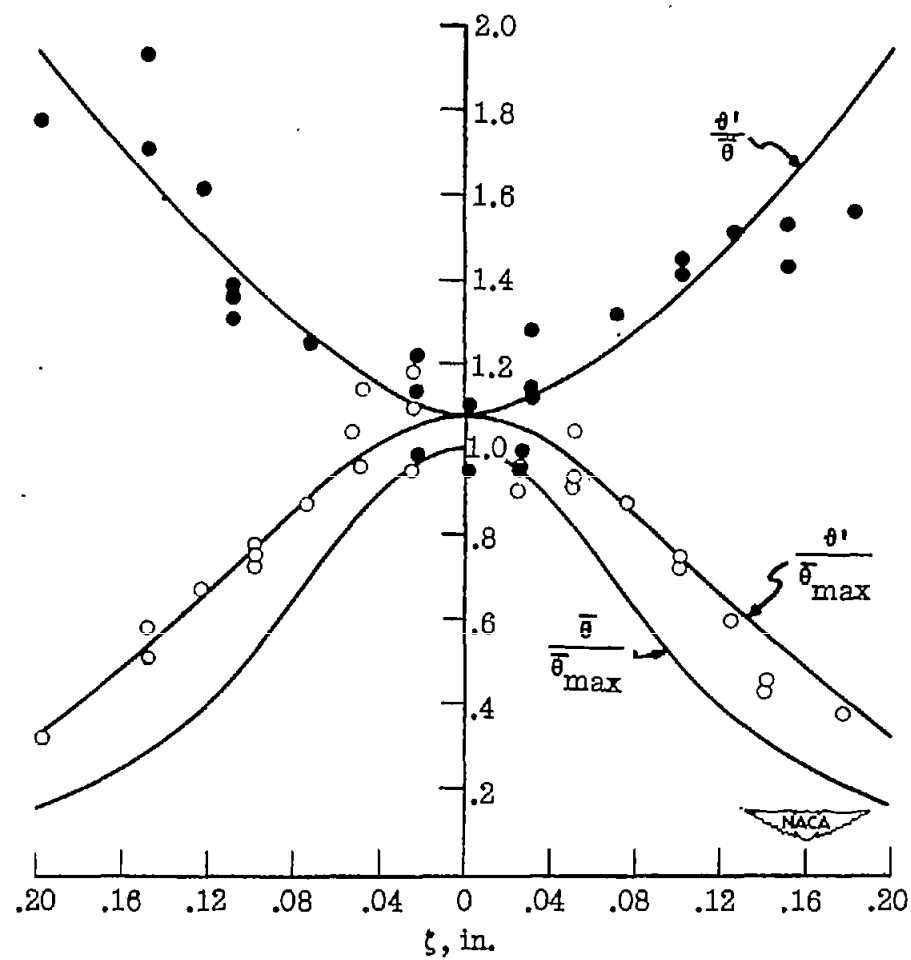


Figure 27.- Temperature fluctuations behind line source of heat in center of unheated jet. $x/d = 20$;
 $\xi = 0.4$ inch.

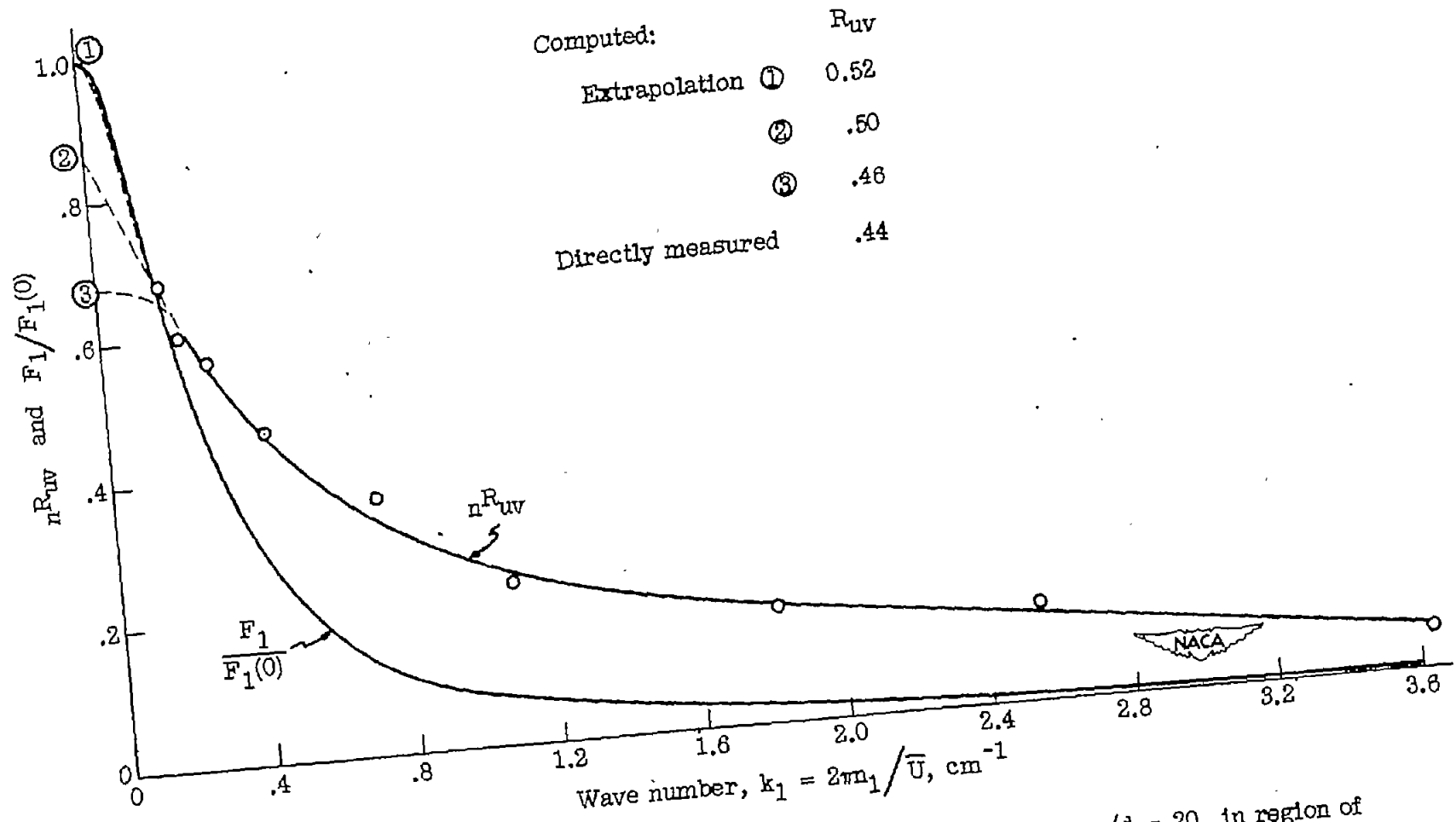


Figure 28.- Shear spectrum and power spectrum in 1-inch unheated jet at $x/d = 20$ in region of maximum shear.

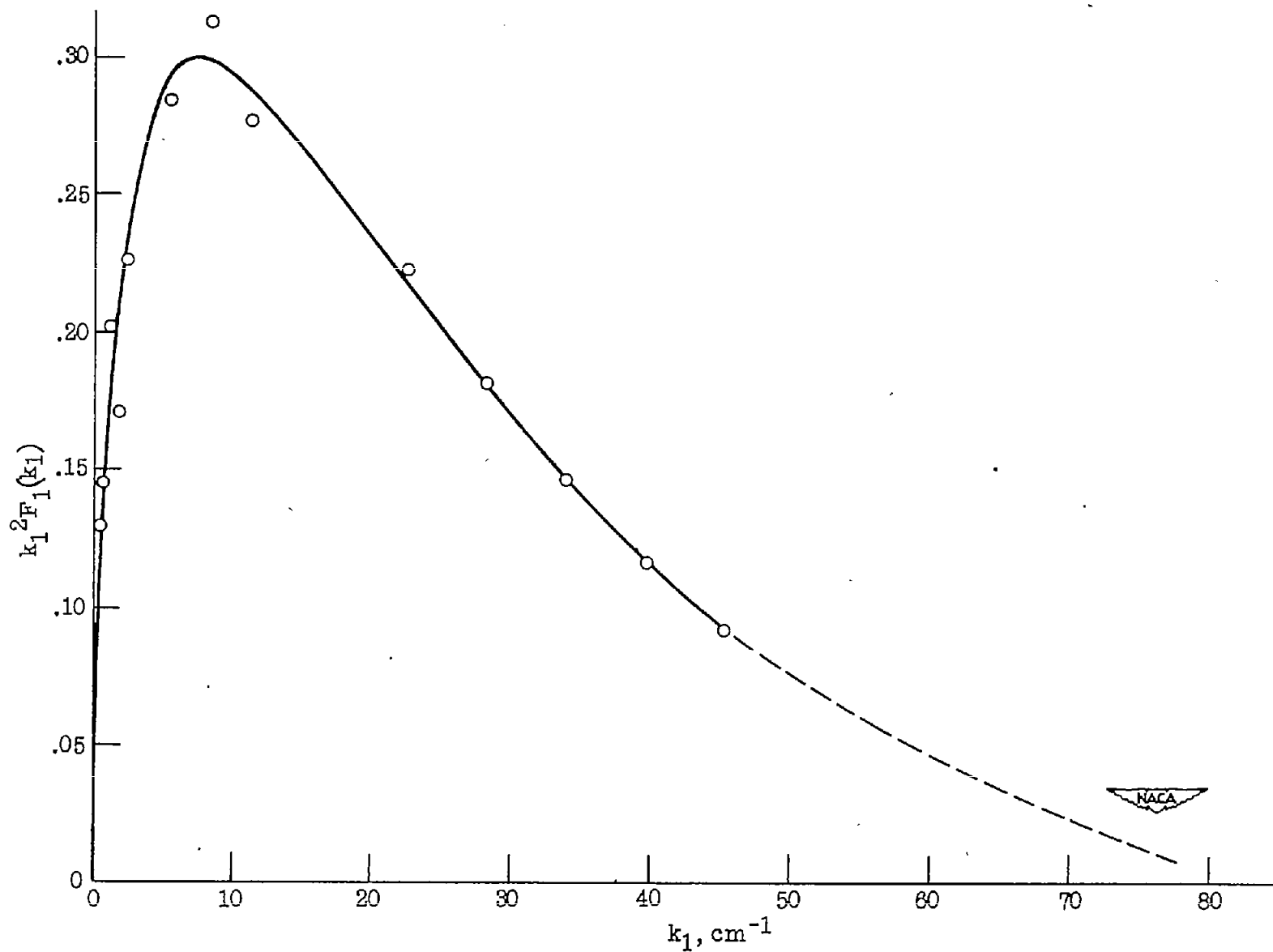


Figure 29.- Viscous dissipation and microscale λ on axis of 1-inch jet. $x/d = 20$; $\frac{1}{\lambda^2} = \int_0^\infty k_1^2 F_1(k_1) dk_1$;
 $\lambda = 0.31$ centimeter.

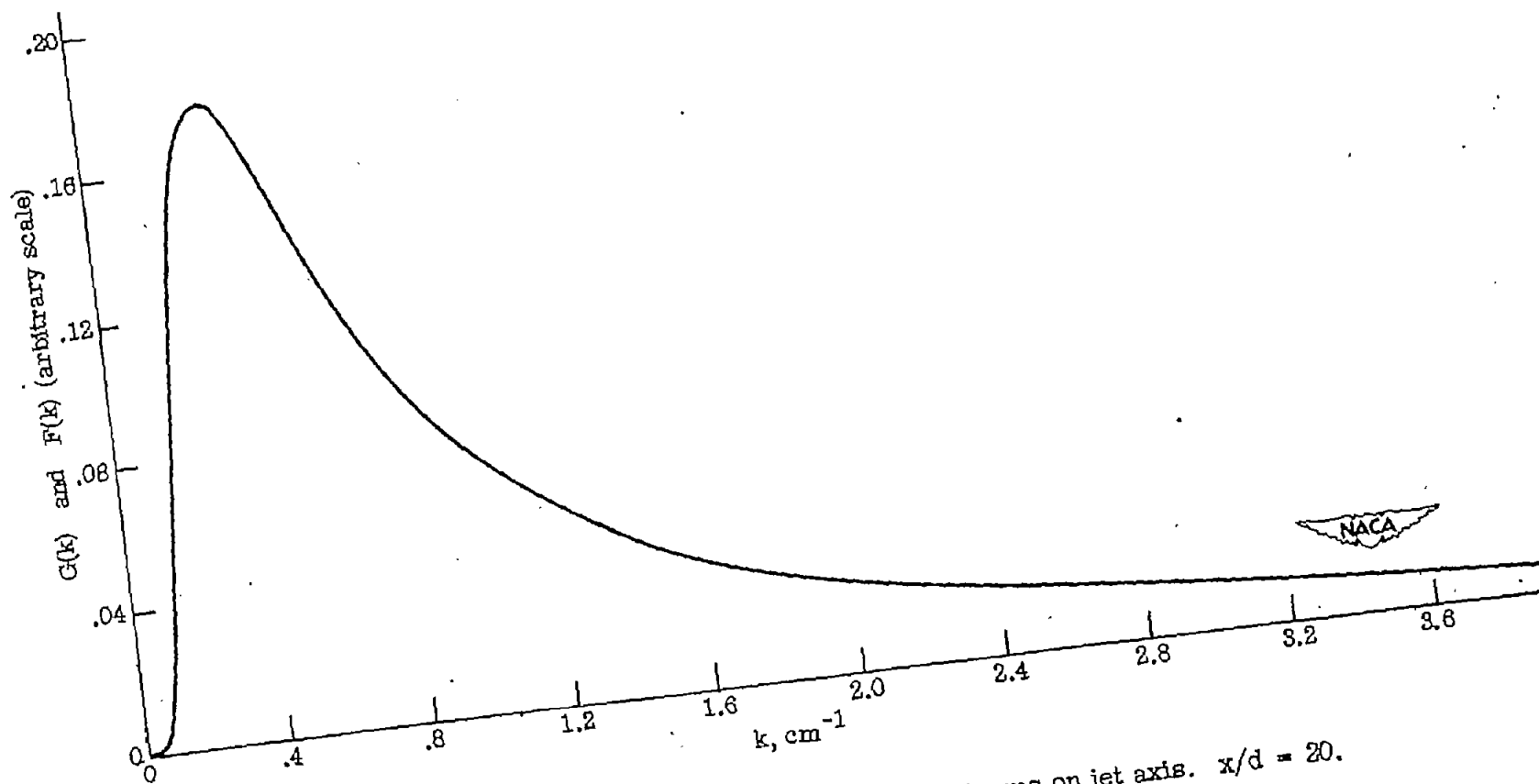


Figure 30.- General nature of three-dimensional spectra on jet axis. $x/d = 20$.

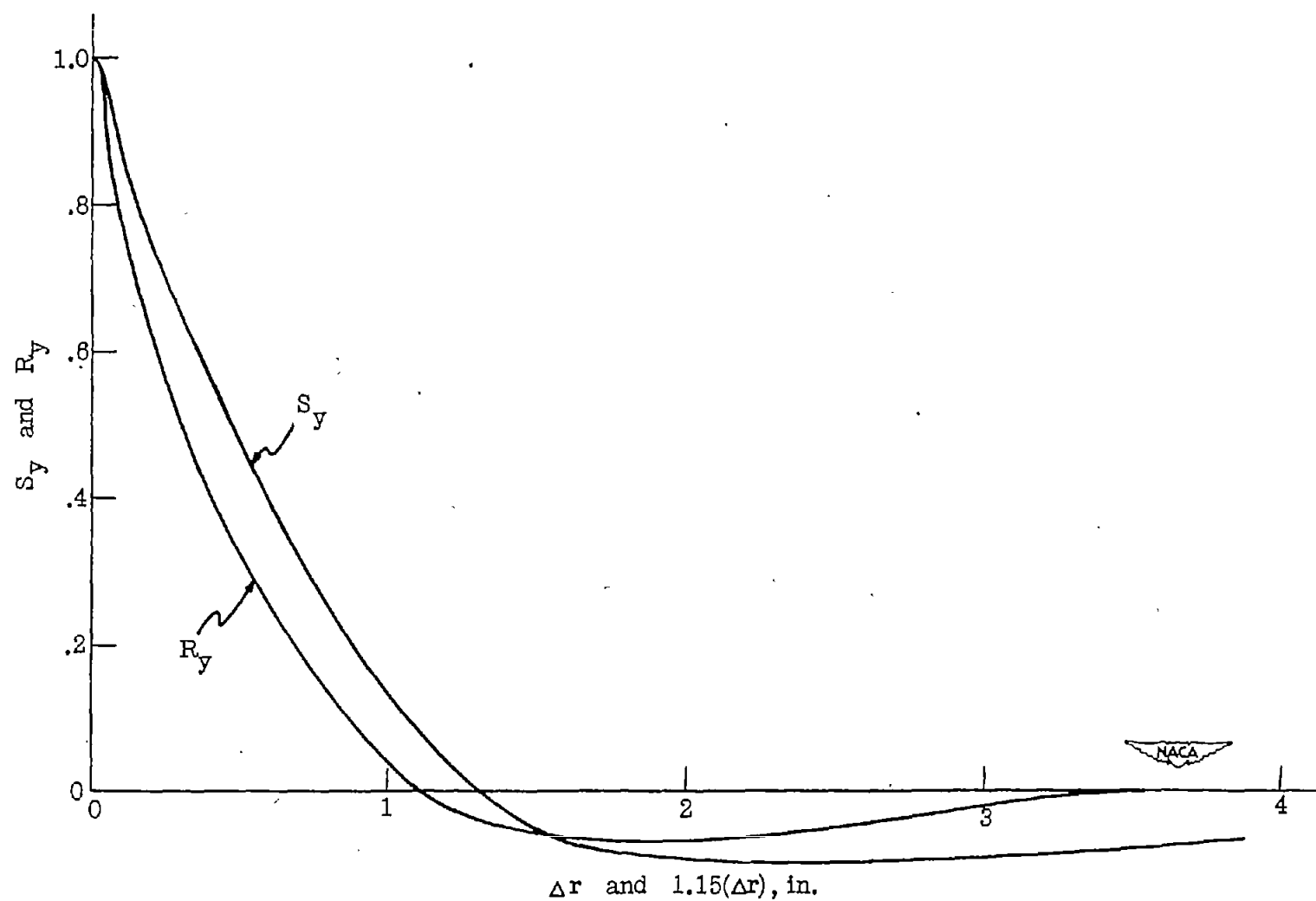
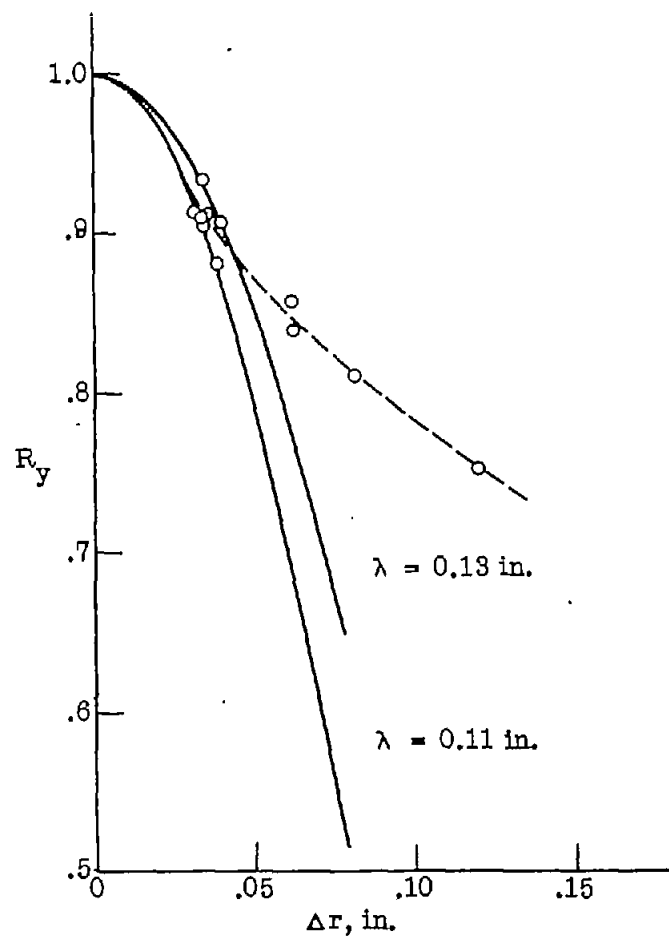
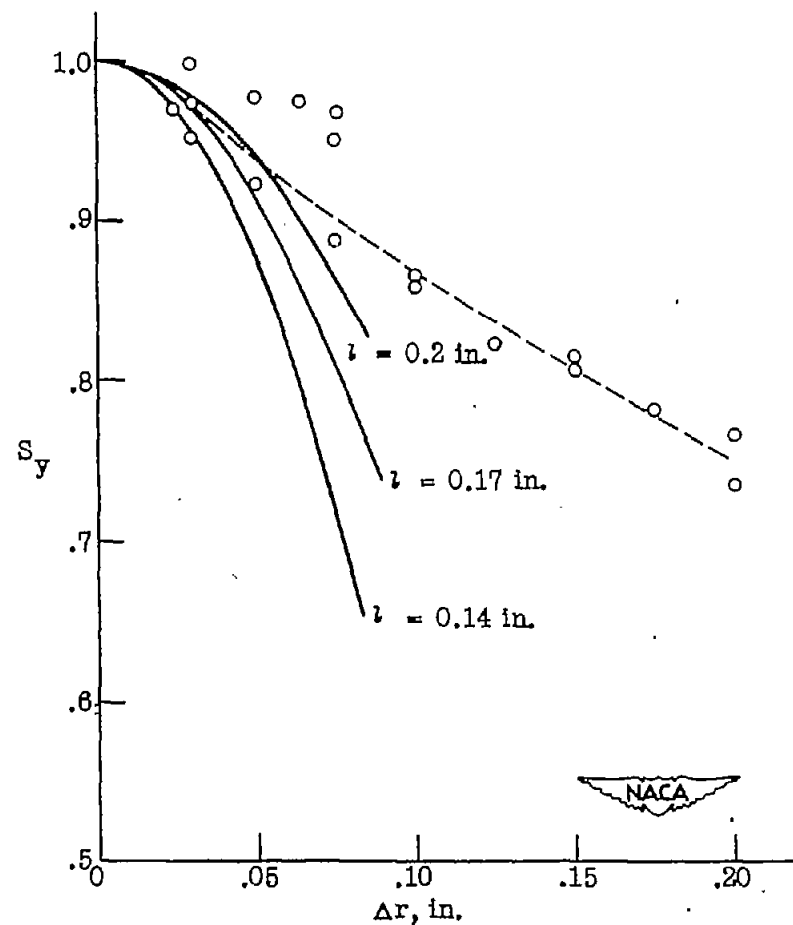


Figure 31.- Comparison of transverse correlation functions. 1-inch heated jet.

(a) Lateral microscale of u -fluctuations.(b) Lateral microscale of θ -fluctuations.Figure 32.- Estimates of microscales. 1-inch jet. $x/d = 20$.

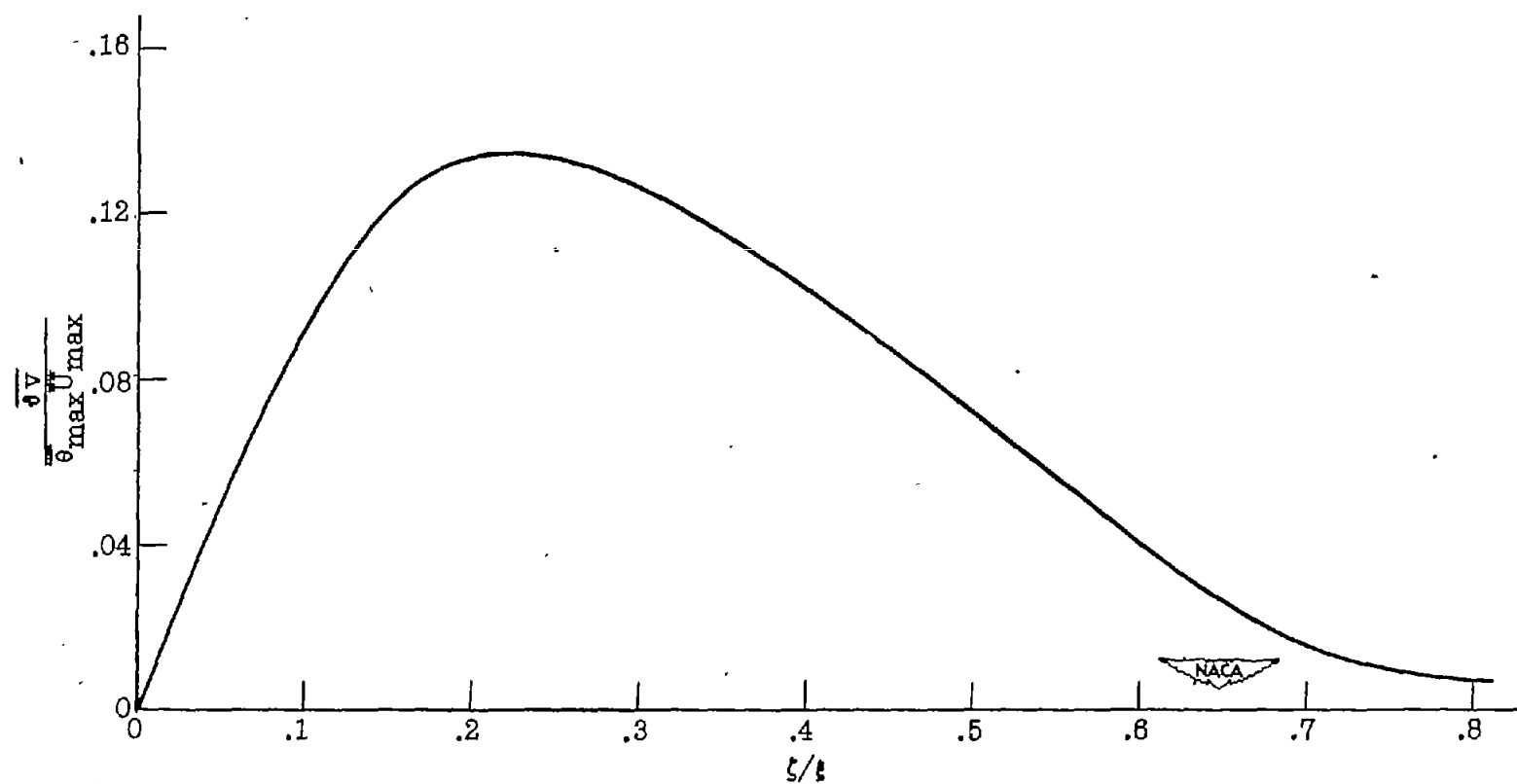


Figure 33.- Thermal wake behind straight-line heat source. Temperature-velocity correlation computed from $\bar{\theta}/\bar{\theta}_{\max}$. $\xi = 0.5$ inch.

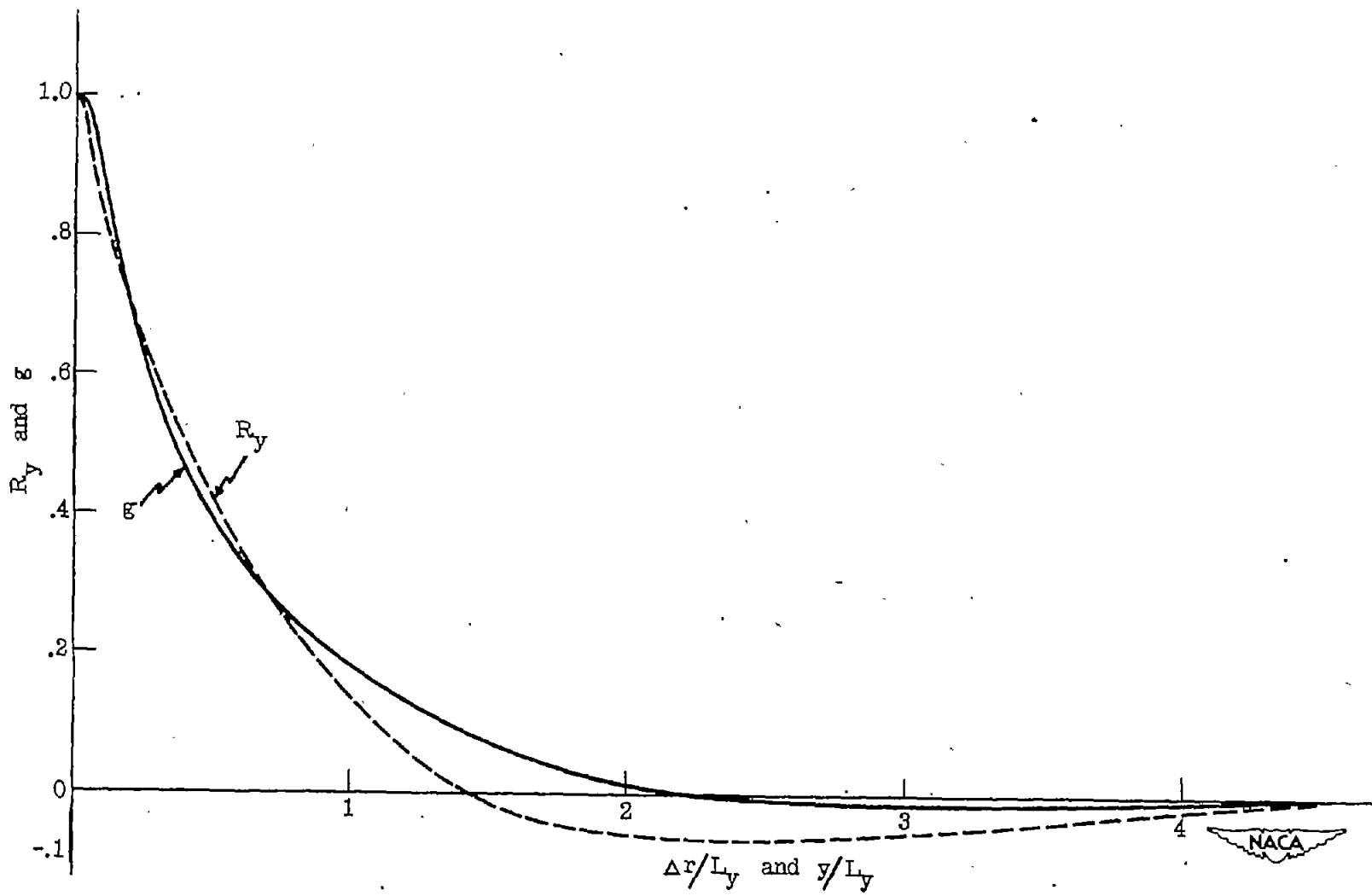


Figure 34.- Transverse velocity correlation functions. $R_y = \overline{u_1 u_2} / \overline{u^2}$ in round jet; $g = \overline{u_1 u_2} / \overline{u^2}$ in isotropic turbulence.

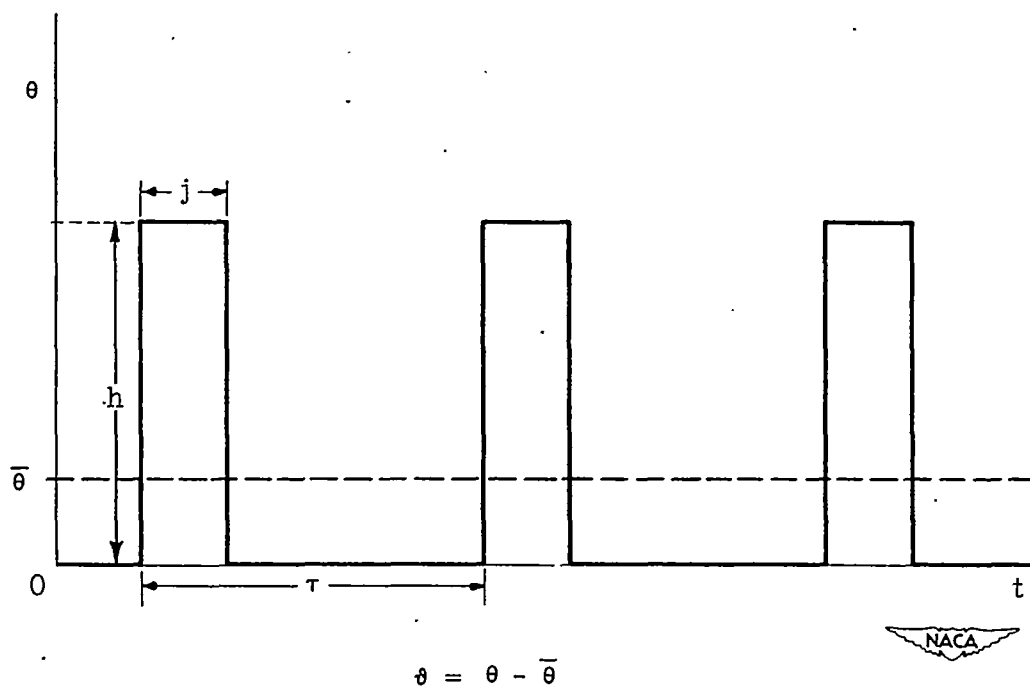


Figure 35.- Simulation of temperature signal close behind local heat source.

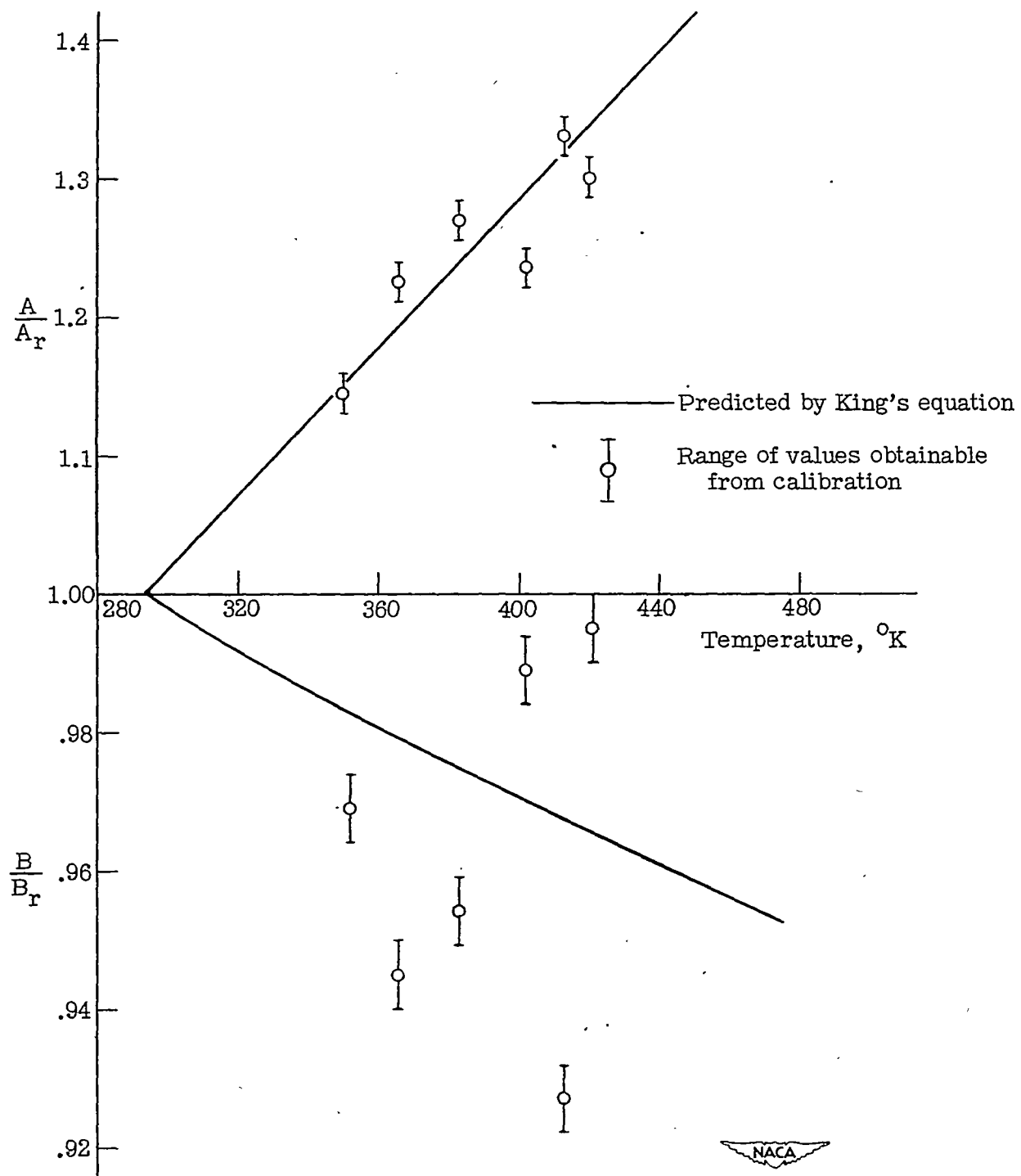


Figure 36.- Variation of hot-wire constants with air temperature.
()_r, room temperature.